# Effect of planetary boundary layer evolution on new particle formation events over Cyprus

Neha Deot[1], Vijay P. Kanawade[1,2*], Alkistis Papetta[1], Rima Baalbaki[3,1], Michael Pikridas[1], Franco Marenco[1], Markku Kulmala[3], Jean Sciare[1], Katrianne Lehtipalo[3,4], Tuija Jokinen[1*]

[1]Climate and Atmosphere Research Center (CARE-C), The Cyprus Institute, Nicosia, Cyprus
[2]Center for Earth, Ocean and Atmospheric Sciences, University of Hyderabad, Hyderabad, India
[3]Institute for Atmospheric and Earth System Research (INAR), University of Helsinki, Helsinki, Finland
[4]Finnish Meteorological Institute, Helsinki, Finland

*Correspondence: Tuija Jokinen (t.jokinen@cyi.ac.cy) and Vijay P. Kanawade (vijaykanawade03@yahoo.co.in)

**Keywords**: New particle formation, planetary boundary layer, free troposphere, mountain environments

**Abstract.**

Atmospheric new particle formation (NPF) occurs ubiquitously in the atmosphere, but more often in the planetary boundary layer (PBL). However, particle formation and early growth are poorly understood processes in aerosol science, particularly over the Eastern Mediterranean and Middle East (EMME) region, which has been recognised as a global climate change hot spot. Here, we present semi-continuous concurrent measurements of ion and particle size distributions in Cyprus for the year 2022 from a lower-altitude rural background site (Agia Marina Xyliatou, AMX, 532 m a.m.s.l.) and a higher-latitude mountain background site (Troodos, TRO, 1819 m a.m.s.l.) with only about 20 km distance between the sites. We also used concurrent measurements of sulfur dioxide, ozone, and meteorological parameters from both sites. The boundary layer evolution and its impact on the occurrence of NPF events at a mountain site were investigated using a combination of water vapour mixing ratio, a passive tracer of PBL dynamics, at both sites and the Vaisala ceilometer estimated and screened PBL height from AMX. We found that NPF event frequencies are comparable between AMX (60%)

and TRO (54%), however only half of the observed NPF events at both sites were observed concurrently. The smaller mode diameter at AMX than at TRO indicates that NPF was initiated near AMX. The observed time for the PBL height to reach the TRO altitude relative to the NPF event start-time at AMX (1.73 hours) is comparable with the time lag between peak particle number concentrations during concurrent NPF events (1.57 hours). Additionally, the growth rates of smaller particles (3–7 nm) were similar, while larger particles (7–25 nm) exhibited higher growth rates at TRO. This suggests that particle growth occurred rapidly in air mass transported from lower altitudes, likely driven by vertical mixing or up-valley winds. Analysis of air mass trajectories supports this interpretation, indicating prior contact of air masses with the PBL before reaching TRO and highlighting the critical role of vertical dynamical mixing in NPF processes. The TRO site is within the PBL for about 25% of days during late winter and early spring, increasing to >80% for the rest of the year, which supports our findings. Our results highlight the significant impact of secondary aerosol production in the evolving PBL on higher-altitude environments, though the vertical extent of nucleation processes remains unclear. Understanding these processes is crucial for climate models, as the PBL drives the exchange of energy, moisture and atmospheric constituents, including aerosols, with the atmosphere above.

## 1. Introduction

Atmospheric new particle formation (NPF) events involve the formation of molecular clusters, via gas-to-particle conversion, from precursor vapours such as sulfuric acid, ammonia, amines, oxidation products of volatile organic compounds, and other trace gases that can form low-volatility complexes, and subsequent growth of these small clusters to larger particles (Kulmala, 2003; Zhang et al., 2004). Globally, NPF is the largest source of aerosol numbers in the atmosphere (Kerminen et al., 2012; Wang and Penner, 2009). These newly formed particles can reach cloud condensation nuclei (CCN) sizes (particle diameter of 50-100 nm and larger) by coagulation and condensation of additional vapours (Kerminen et al., 2018; Sebastian et al., 2022; Pierce and Adams, 2009; Westervelt et al., 2013; Williamson et al., 2019). Global modelling simulations showed that NPF events produce half of the present-day global CCN number (Merikanto et al., 2009; Spracklen et al., 2008; Westervelt et al., 2014; Yu and Luo, 2009), with an estimated uncertainty range from 38 to 66% (Gordon et al., 2017). The uncertainty in CCN production in the global climate model itself stems partly from the uncertainty in particle formation and growth (Ipcc, 2023). Additionally, human exposure to inhalable fine particles, from both primary and secondary sources, has serious health risks that can lead to premature death (Lelieveld et al., 2019).

To date, there are a scanty number of studies investigating characteristics of NPF events over Cyprus (Baalbaki et al., 2021; Brilke et al., 2020; Debevec et al., 2018; Gong et al., 2019) and overall the limited number of studies over the EMME region (Aktypis et al., 2023; Aktypis et al., 2024; Dinoi et al., 2023; Hakala et al., 2019; Hussein et al., 2020; Hakala et al., 2023; Pikridas et al., 2012; Kalkavouras et al., 2019; Kalivitis et al., 2019; Kalkavouras et al., 2020; Kalkavouras et al., 2021; Manninen et al., 2010). The EMME region is characterised by diverse air masses originating from continental, maritime, and desert areas, which affect the atmospheric composition and climate in the area (Bimenyimana et al., 2023; Vrekoussis et al., 2022; Zittis et al., 2022). While NPF events have been frequently observed in western Saudi Arabia without any clear seasonal pattern (Hakala et al., 2019), Hussein et al. (2020) observed the highest NPF event frequency during summer in Amman, Jordan. In contrast, NPF events were frequently observed during spring and autumn in the eastern Mediterranean (Baalbaki et al., 2021; Kalivitis et al., 2019). The frequent occurrence of NPF events in the eastern Mediterranean has been linked to various factors, such as solar radiation/temperature, terrestrial biogenic activity, higher sulfuric acid ($H_2SO_4$) concentrations, high-dust episodes, and/or air mass history, but it is still not completely clear what drives the frequent occurrence of NPF events over this region (Baalbaki et al., 2021). A previous study showed that NPF events occurred on 58% of days annually at a lower-altitude site, Agia Marina Xyliatou (AMX) (Baalbaki et al., 2021), which is the highest reported frequency after South Africa (86%) (Hirsikko et al., 2012) and Saudi Arabia (73%) (Hakala et al., 2019). In contrast, NPF events occurred only on 12% of days during summer at a higher-altitude mountain site (Helmos mountain at 2314 m a.m.s.l.) in Greece (Aktypis et al., 2024). Previous studies have shown that NPF events at higher-altitude locations occur under the influence of up-valley winds, which channel precursor gases to higher altitudes, typically when the boundary layer extends above the site's altitude (Bianchi et al., 2016; Tröstl et al., 2016a; Sebastian et al., 2021), and NPF events were observed even at higher vapour condensation sink compared to non-events (Sellegri et al., 2019). On the contrary, Boulon et al. (2011) showed that NPF events were observed more frequently in the free troposphere (43.5% of the total observation days at the Puy de Dôme station, 1465 m a.m.s.l.) than within the planetary boundary layer (PBL) lower-altitude (2.5% of the total observation days at the Opme station, 660 m a.m.s.l.) in Central France.

Boundary layer NPF phenomena have extensively been studied worldwide (Nieminen et al., 2014; Kerminen et al., 2018; Nieminen et al., 2018; Lee et al., 2019; Kulmala et al., 2004), although up to which altitude NPF events take place in the PBL, and where they are initiated is still unclear (Wehner et al., 2010; Stratmann et al., 2003; Minguillón et al., 2015). Minguillón et al. (2015) demonstrated that intense NPF events in Barcelona primarily occur at a surface level around midday, coinciding with high insolation and pollution dilution, whereas early-morning NPF events are constrained to higher altitudes due to the inhibition of these events by high surface-level condensation sink (CS). Carnerero et al. (2018) demonstrated that ultrafine particles are formed exclusively inside the mixed layer, and as the mixed layer grows, ultrafine particles are detected at higher levels within PBL, while Wehner et al. (2010) observed well-mixed ultrafine particles (5-10 nm) throughout the PBL. A one-dimensional coupled column model, SOM-TOMAS (Statistical Oxidation Model of organic chemistry and Two Moment Aerosol Sectional microphysics model), demonstrated that enhanced NPF rates in the upper mixed layer are strongly influenced by temperature, vertical mixing, and gas-phase precursor concentrations (O'donnell et al., 2023). Aircraft observations over boreal forests showed that particle concentrations (>1.5 nm) peak near the surface in the morning and mix within the evolving PBL layer during the day (Leino et al., 2019). However, airborne observations are costly and operationally challenging. Our sites offer a unique opportunity to study the vertical extent of NPF events and aerosol populations within the PBL, due to their close proximity, and the mountain background site (TRO) is within the PBL for about >80% of days during the year. The intense solar radiation, the intricate mixture of both natural and anthropogenic emissions from continental and marine origins, the presence of local breeze systems (mountain, valley, sea, and land) and elevated dust layers further add complexity to the PBL–NPF relationship over the region. The combination of these factors poses a significant challenge in understanding the drivers behind the frequent NPF events observed in Cyprus and, more broadly, across the Eastern Mediterranean.

In this work, we used semi-continuous concurrent measurements of ion and particle size distributions for the year 2022 from a lower-altitude rural background site (AMX) and a higher-altitude mountain background site (TRO) in Cyprus with a 1287 m difference in altitude in 20 km distance between the observational sites. We present analysis on concurrent and individual (i.e. an event happening only at one site while the other site did not show an event) NPF events.

The main aim is to examine the effect of PBL evolution on NPF events at a background mountain site in Cyprus.

## 2. Materials and methods

### 2.1 Measurement Sites

The Eastern Mediterranean and Middle East region has been recognized as a global climate change hotspot, which serves as a convergence zone for air masses originating from three distinct continents (Europe, Asia, and North Africa), including marine, anthropogenic, and desert dust sources. AMX and TRO are sites of the Cyprus Atmospheric Observatory (CAO) network, operated by the Climate and Atmosphere Research Center (CARE-C) of the Cyprus Institute. The AMX site (35.038692° N, 33.057850° E) is located at 532 m a.m.s.l. between two villages, Agia Marina Xyliatou and Xyliatos, at the foothills of the Troodos mountain range in the central Republic of Cyprus. The AMX site is located about 1.5 km South of Agia Marina Xyliatou and about 2.2 km Northeast of Xyliatos. The AMX site hosts instruments affiliated with several research infrastructures such as the cooperative program for monitoring and evaluation of the long-range transmission of air pollutants in Europe (referred to as the European Monitoring and Evaluation Programme, EMEP), the air quality network of Cyprus operated by the Department of Labour Inspection (DLI), regional Global Atmospheric Watch (GAW) program of the World Meteorological Organization (WMO), the Aerosols, Clouds and Trace Gases Research Infrastructure (ACTRIS) aerosol in situ network, e-Profile (part of EUMETNET), and NASA's AERosol RObotic NETwork (AERONET). Anthropogenic emissions in the vicinity of the AMX site are minimal and the major cities are located at about 35 km (Nicosia) to the Northeast and about 50 km (Larnaca) to the Southeast.

The TRO site (34.9430333° N, 32.8654729 E) is located at 1819 m a.m.s.l., close to Mount Olympus (the highest peak of Cyprus, 1952 m a.m.s.l.) and experiences free tropospheric conditions, primarily during winter. TRO site may also experience light to moderate snowfall during winter, usually in January and February, and it is in cloud sporadically. The site is considered a background higher-altitude mountain location as it has little or no influence from local anthropogenic activities, except occasional camping or campfire activities in the vicinity and the staging post for helicopter operations. Small villages such as Prodromos, Palaiomylos, and Agios Dimitrios are located to the West of the TRO site, while the Troodos village is located to the Southeast within a 5 km distance. It is located centrally with respect to the major cities: Limassol, about 36 km to the South, Paphos, 42 km to the Southwest, Nicosia, 50 km to the Northeast, and Larnaca, 70 km to the Southeast. Figure 1 shows the surface elevation map of Cyprus depicting the locations of AMX and TRO sites and pictures of the AMX and TRO site premises.

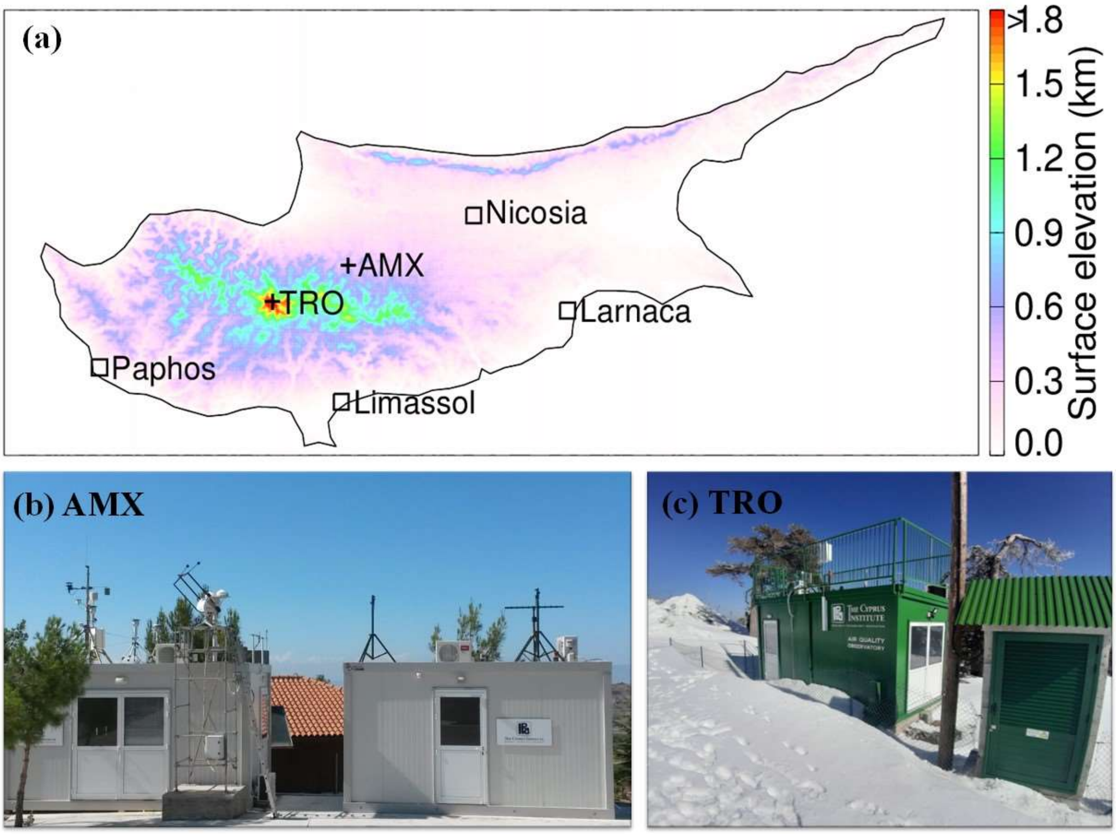


**Figure 1**. (a) Surface elevation map of Cyprus, including the location of AMX and TRO observational sites and the major cities. Elevation data is obtained from the U.S. Geological Survey global digital elevation model (DEM) with a horizontal grid spacing of 30 arc seconds (approximately 1 km (GTOPO30). (b) and (c) show AMX and TRO site premises pictures, respectively.

## 2.2 Instrumentation

### *2.2.1 Neutral Cluster and Air Ion Spectrometer (NAIS)*

The ion and total particle number size distributions were measured using the NAIS (Airel Ltd. Estonia) at both measurement sites to detect and characterise NPF events. The NAIS measures the number size distribution of ions and naturally charged particles in the diameter range of 0.8 – 42 nm for NTP conditions (mobility range: 3.162 – 0.0013 $cm^2\ V^{-1}\ s^{-1}$) (Mäkelä et al., 1996), simultaneously in both positive and negative polarity (Manninen et al., 2016; Mirme and

Mirme, 2013). Additionally, the NAIS can measure the total particle size distribution by using corona charging. Briefly, the NAIS has two parallel cylindrical differential mobility analysers (DMAs): one classifies positively charged ions, and the other classifies negatively charged ions. The air is sampled at a flow rate of 54 L min$^{-1}$, with a sampling tube inner diameter of 30 mm and a length of 65 cm. Subsequently, the airflow is divided equally for each polarity before entering the preconditioning unit. Here, depending on the operational mode, the aerosol samples either pass through without modification (ion mode), or they are charged to the same polarity of the analysers (particle mode) or they are charged to the opposite polarity of the analyser (offset mode). The air sample then reaches the analysers, where it is size-classified in an electrical field and detected by electrometers. The total particle concentration below ~2 nm cannot be detected due to the ions produced by the corona charger itself, and therefore discarded in the data analyses. The NAIS SPECTOPS software with an instrument-specific algorithm was used to invert the raw counts into a size distribution. The inverted data was subsequently corrected for line losses using the Gormley and Kennedy equation for inlet line losses for laminar flow (Gormley and Kennedy, 1949). Note that NAIS data is available for approximately 60% and 63% of the days at AMX and TRO, respectively (Fig. S1), which is statistically robust for this analysis.

### *2.2.2 Ceilometer CL51*

The Vaisala Ceilometer CL51 is part of the E-PROFILE network, operational since 2021 which coordinates the measurements of vertical profiles of wind, aerosol, and clouds from radars, lidars, and ceilometers from a network of locations across Europe and provides the data to the end users. The Vaisala Ceilometer CL51 utilises an eye-safe indium gallium arsenic (IngAas) diode-laser lidar technology, emitting 110 ns-long pulses with a wavelength of 910±10 nm and a repetition rate of 6.5 kHz in a vertical or near-vertical direction (Münkel and Roininen, 2010). The CL51 can measure aerosols and clouds from above the overlap region ~300 m up to 15 km nominally, with a vertical resolution of 10 m. The backscatter profile is used to identify up to three aerosol-layer heights using the gradient method in the postprocessing software provided by the manufacturer (BL-VIEW), which includes an automated mixing height detection algorithm described by Emeis et al. (2007). The VAISALA BL-VIEW software features a “cloud and precipitation filter” known as the enhanced gradient method (Münkel and Roininen, 2010), which filters out high backscatter signals from clouds and precipitation before applying the gradient method. BL-View’s calculation is based on the combined gradient and idealised backscatter methods that enable reliable automatic estimation of the PBL height (PBLH) at a temporal resolution of 16 seconds and a vertical resolution of 10 m. Here, we used Level 3 boundary layer height data with a quality control index of "good" only.

### *2.2.3 Ancillary measurements*

We used aerosol optical depth (AOD) and angstrom exponent (AE) data from the AERONET sunphotometers at both AMX and TRO sites. Trace gas concentrations, such as sulfur dioxide ($SO_2$) and ozone ($O_3$), and the meteorological parameters (temperature, relative humidity, solar radiation, wind speed, and wind direction) at AMX station were taken from the air quality network of Cyprus operated by the DLI. At the TRO site, TELEDYNE gas analysers for $SO_2$ (Model T100U) and $O_3$ (Model T400) were deployed and meteorological parameters were obtained from the Department of Meteorology automatic weather station, located about 3.3 km south of the measurement site. Note that all data is reported in Universal Time Coordinated (UTC). Local time in Cyprus is UTC+2 from late October to late March (Eastern European Time) and UTC+3 from late March to late October during daylight saving time (Eastern European Summer Time). We have used quality-assured and quality-controlled data using standard procedures and instrument data quality flags.

## 2.3 Tracers used to investigate PBL evolution

We used two distinct methods to investigate how often the mountain background site, TRO, is influenced by PBL evolution. First, the water vapour mixing ratio (WVMR) at TRO was used to distinguish between free tropospheric and PBL air. A threshold WVMR value of 5.25 g/kg (which is the $30^{th}$ percentile value of WVMR at the AMX site) was used, with WVMR values below 5.25 g/kg indicating free tropospheric air (Zha et al., 2023). WVMR was calculated as follows:

$$WVMR = B \times \frac{e}{p - e} \qquad (1)$$

where B is a constant (621.9907 g $kg^{-1}$, molecular weight ratio of water to dry air), e and p are the water vapour pressure and the atmospheric pressure, respectively. e was calculated using ambient temperature, RH, and pressure (Buck, 1981).

Secondly, the Vaisala ceilometer estimated PBLH from the AMX site was used to examine the PBL evolution up to the altitude of the TRO site. The PBLH estimation algorithm might be influenced by boundary layer stability, near-surface or elevated aerosol layers, moving cloud systems in the vicinity of the measurement site, and surface type. Zhang et al. (2022) showed that the ceilometer estimated PBLH generally compares well with the bulk Richardson number method under stable conditions. ERA5 also used the bulk Richardson number method to calculate PBLH (Hersbach et al., 2020). Therefore, we apply a robust data filtering technique to remove under or over-estimated PBLH data values in conjunction with ERA5 PBLH data (Hersbach et al., 2023), the latest version of ECMWRF reanalysis, which is available on a 1440 × 721 longitude and latitude grid, with a spatial resolution of $0.25^o \times 0.25^o$ and a temporal resolution of 1 hour. First, we remove ceilometer estimated PBLH which is lower or greater than three standard deviations of PBLH for a given day. Second, we used ERA5 PBLH to match the diurnal pattern and considered only those days when the correlation coefficient between ERA5 and Ceilometer PBLH was greater than 0.5 at a statistical significance level of 95%. After applying these constraints, we retained 5688 hourly data points from a total of 7248 valid hourly data points, thereby ensuring that only the most reliable data were included in the PBLH analysis.

### 2.4 Event classification

The traditional ways to classify the given day into different types of NPF events (Dal Maso et al., 2005; Hirsikko et al., 2007; Kulmala et al., 2012; Manninen et al., 2010) are mainly based on the visual appearance of a contour plot of particle number size distributions. A day with the appearance of a new particle mode followed by its growth is identified as an NPF event day and such events occur over a spatial scale of a few 100's kilometres and a temporal scale of 1-2 days and are thus referred to as regional NPF events. The downside of these methods is a large fraction of unclear days, which could be caused by more local NPF events, changes in air masses, or varying weather conditions. Such unclear events can also be further classified into different sub-classes (nucleation-mode peak, Aitken-mode, and tail), but it requires additional information on trace gases and aerosol characteristics (Kanawade et al., 2014; Buenrostro Mazon et al., 2009). However, the data analysis becomes more complex when these unclear days form a large fraction of all the days. In addition, these methods omit potentially low-intensity NPF events such as local or short-lived NPF events (Kulmala et al., 2024). Here, we used the traditional methodology for classifying a given day into NPF event, non-event and unclear. Given the asynchronous data gaps in NAIS measurements at both sites, we introduced an additional category labelled 'nodata,' which must be considered when comparing the frequency of occurrence of different event types. nodata days include the unavailability of the instrument, maintenance (mainly the cleaning of the instrument during the summer and dust episodes), troubleshooting of the instrument, and infrequent power cuts at the measurement site. We present the frequency of occurrence for all these event types and utilise only NPF events for data analysis in this work.

### 2.5 Air mass history analysis

Three-day backward airmass trajectories arriving at 1000 m a.m.s.l. and 2000 m a.m.s.l. to AMX and TRO, respectively, during 6 - 12 UTC were determined using the National Oceanic and Atmospheric Administration (NOAA) ARL PC-version HYbrid SingleParticle Lagrangian Integrated Trajectory (HYSPLIT) transport and dispersion model (Draxler and Rolph, 2010), using 0.25 degree gridded wind fields from the Global Forecast System (GFS).

## 3 Results and Discussion

### 3.1 NPF event frequency and characteristics

The temporal evolution of negative ion and particle number size distributions at both sites (AMX and TRO) for the year 2022 are shown in Fig S1. Ion and particle number concentrations are generally higher at AMX than at TRO. Figure 2 shows the concurrent evolution of negative ion and particle number size distributions and number concentrations for observed typical NPF events at both sites and PBLH at the AMX site from 28 - 30 April 2022. The negative ion and particle number concentrations are two-fold higher at the AMX site as compared to the TRO site. While larger diameter background particles were continuously present at the AMX site, they were absent at the TRO site, suggesting that NPF events may be the major source of larger diameter particles in the Aitken mode at the TRO site (Fig. 2 and S1). Furthermore, the banana-shaped aerosol formation and growth pattern were significantly broader below 10 nm at the AMX site compared to the TRO site, suggesting that the intense NPF most likely lasted longer and the precursor vapour supply was sustained for a longer duration at AMX than at TRO. The PBLH was higher than the altitude of the TRO site, possibly indicating that the concurrent occurrence of NPF events at TRO was influenced by the evolution of the PBL (see section 3.3).

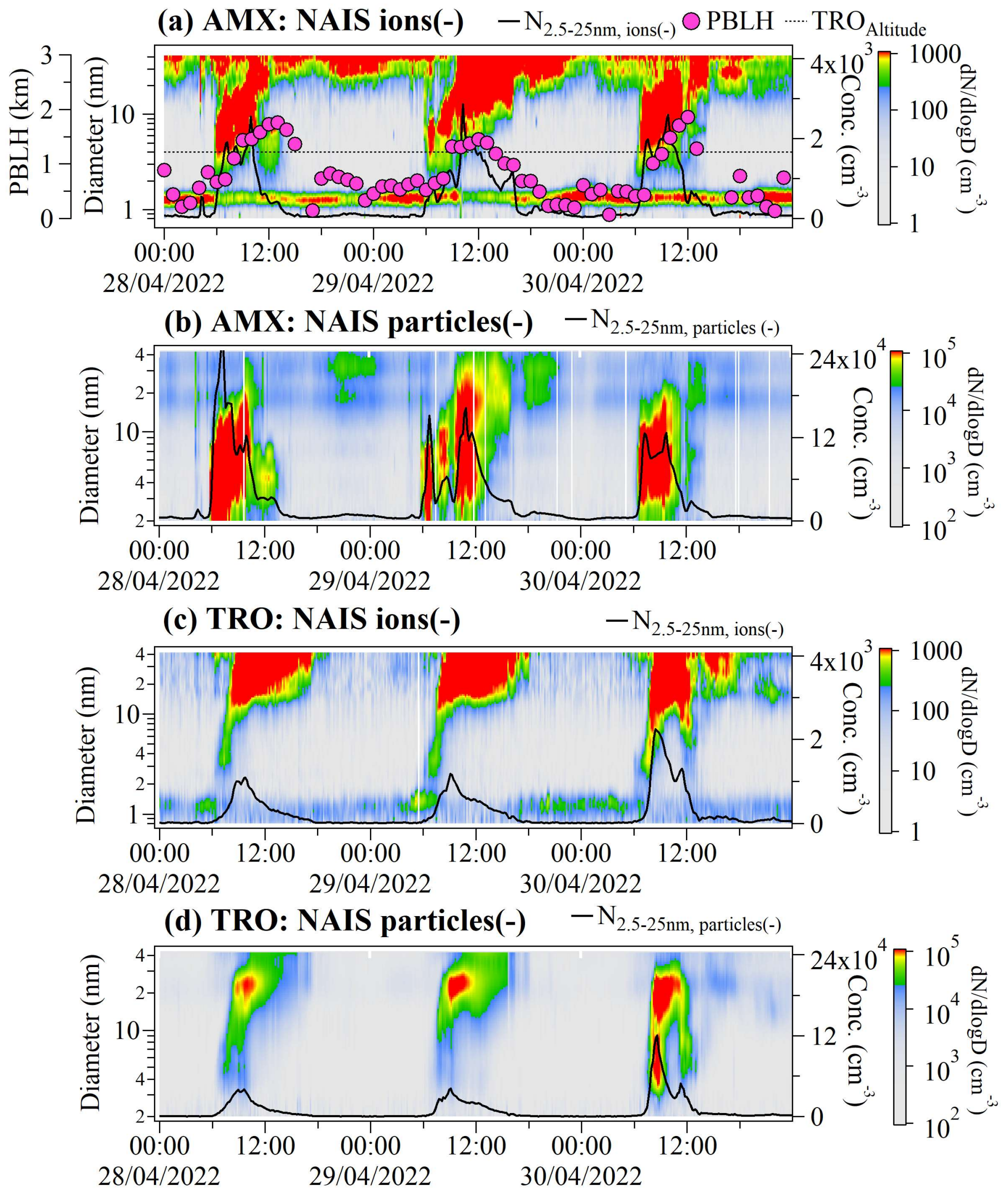


**Figure 2**. Time evolution of 10-minute averaged number size distributions of negative polarity ions and total particles at AMX (a, b) and TRO (c, d), respectively, measured with NAIS from 28 April to 30 April 2022. The ion and particle number concentrations in the mobility diameter range from 2.5 to 25 nm are shown by a solid black line. The PBLH at AMX above the ground and the altitude of the TRO site above AMX are indicated by magenta colour dots and a black colour dotted line, respectively.

Figure 3a shows the occurrence frequency of different types of event days at both AMX and TRO sites. At AMX, NPF events were observed on 129 days (35.34%), 43 days did not have signs of NPF (non-events, 11.78%), while 42 days (11.51%) were unclear and there were no valid measurements on 151 days (41.37%) during the calendar year of 2022. At TRO, NPF events were observed on 121 days (33.16%), 39 days did not show NPF (non-events, 10.68%), 64 days were unclear (17.53%), and there were no valid measurements on 141 days (38.63%). Out of the total observed NPF events at AMX (129 days out of 214 valid observation days, 60%) and at TRO (121 days out of 224 valid observation days, 54%), NPF events were observed concurrently on 69 days at both sites (Table S1), indicating that the remaining NPF events occur in different air masses at these sites even with the close proximity of sites (approximately 20 km). The NPF frequency at the AMX site was the highest during spring as compared to the rest of the year, analogous to the previous study at AMX (Baalbaki et al., 2021) and other closest Eastern Mediterranean site, Finokalia atmospheric observation station, in Crete (Kalivitis et al., 2019). The NPF frequency at the TRO site appears to be the highest during spring, although the NPF frequency in July was comparable. The gaps in observational data limit a detailed discussion of the seasonal characteristics of NPF events at both sites, however, the concurrent observations, covering over 60% at both sites, are sufficient to assess the impact of PBL evolution on NPF events at the TRO site.

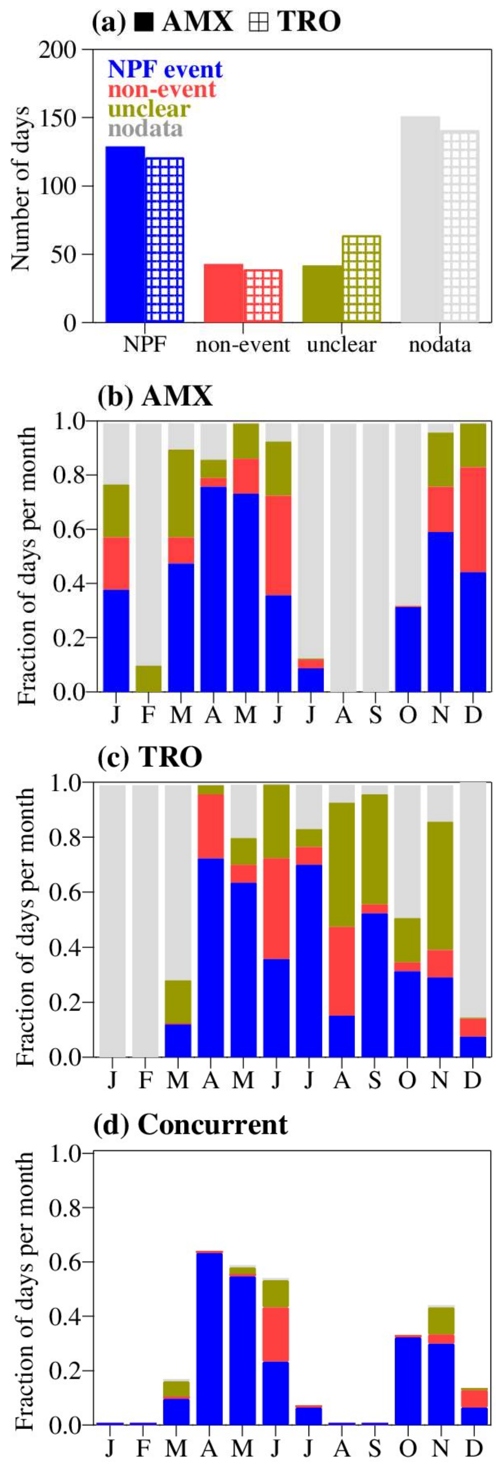


**Figure 3**. (a) Number of days of different event types at both AMX and TRO sites, (b) occurrence frequency (in fraction of days per month calculated as the number of event days divided by the total number of calendar days in the month) of different event types at AMX, (c) same as (b) but for TRO, and (d) same as (b) but for concurrent days of NPF events, non-events and unclear days at both AMX and TRO sites, excludes individual different events types and nodata.

## 3.2 Diurnal variation in negative polarity size-segregated ion and total particle number concentrations, NPF events start-time and mode diameter

Figure 4 shows the diurnal variation of size-segregated ion and particle number concentrations for negative polarity (see Fig. S2 for positive polarity) for concurrent NPF events observed at both sites as well as NPF events observed individually at each site. We used four size classes: 2.5-7 nm, 7-25 nm, 2.5-25 nm, and >2.5 nm for both ions and particles. Ion and particle number concentrations exhibit similar diurnal cycles, with the highest concentrations occurring between 06:00 and 14:00 UTC, as NPF is predominately a daytime phenomenon driven by photochemistry in the presence of solar radiation (Asmi et al., 2011; Jokinen et al., 2017; Kanawade et al., 2012; Kerminen et al., 2018; Z. Wu et al., 2007). The noontime peak in size-segregated ion and particle number concentrations indicates the importance of photochemistry for NPF events at AMX and TRO sites. The concurrent peaks in temperature (Fig. S3a), solar radiation (Fig. S3b) and sulfur dioxide (Fig. S3c) during NPF events are also visible. The low relative humidity (Fig. S3d), higher ozone concentrations (Fig. S3e), and lower wind speed (Fig. S3f) further indicate environmentally favourable conditions to promote particle formation and growth. Seasonally averaged diurnal patterns of columnar aerosols (AOD) during spring, summer and autumn closely resemble one another (probably indicating that TRO is influenced by the PBL evolution) with higher aerosol loading at AMX compared to TRO (Fig. S4a), whereas they do not align well in winter (TRO is weakly influenced by the PBL evolution). Additionally, the higher Ångström exponent at TRO (Fig. S4b), particularly in winter when the TRO mostly lies in the free troposphere (see section 3.3), suggests that these small particles are likely from local primary emissions (traffic, residential, etc.) or airborne secondary production or both. Furthermore, the absence of traffic-induced morning and evening peaks in size-segregated ion and particle number concentrations suggests that both sites are not influenced by local traffic emissions (Fig. 4). The blue and red vertical lines in Figure 4 indicate the occurrence times of peak concentrations for concurrent NPF events at AMX and TRO, respectively. The peak was consistently shifted to the right at the TRO site, except for intermediate ions (2.5–7 nm). This shift suggests a temporal delay of NPF events compared to AMX. This variation could reflect differences in local atmospheric dynamics, such as PBL evolution alongside aerosol precursors required for aerosol formation and growth. When mountain sites experience daytime evolution of the PBL, a similar diurnal cycle of aerosol properties, to that of lower-altitude sites, is typically observed (Collaud Coen et al., 2018). Therefore, we hypothesise that the NPF event is detected earlier at the AMX site, shortly after sunrise, coinciding with an increase in temperature that drives the evolution of the PBL up to the height of the TRO site. The evolution of the PBL may carry precursor gases and aerosols up to the TRO site altitude, resulting in a later starting time of NPF events there.

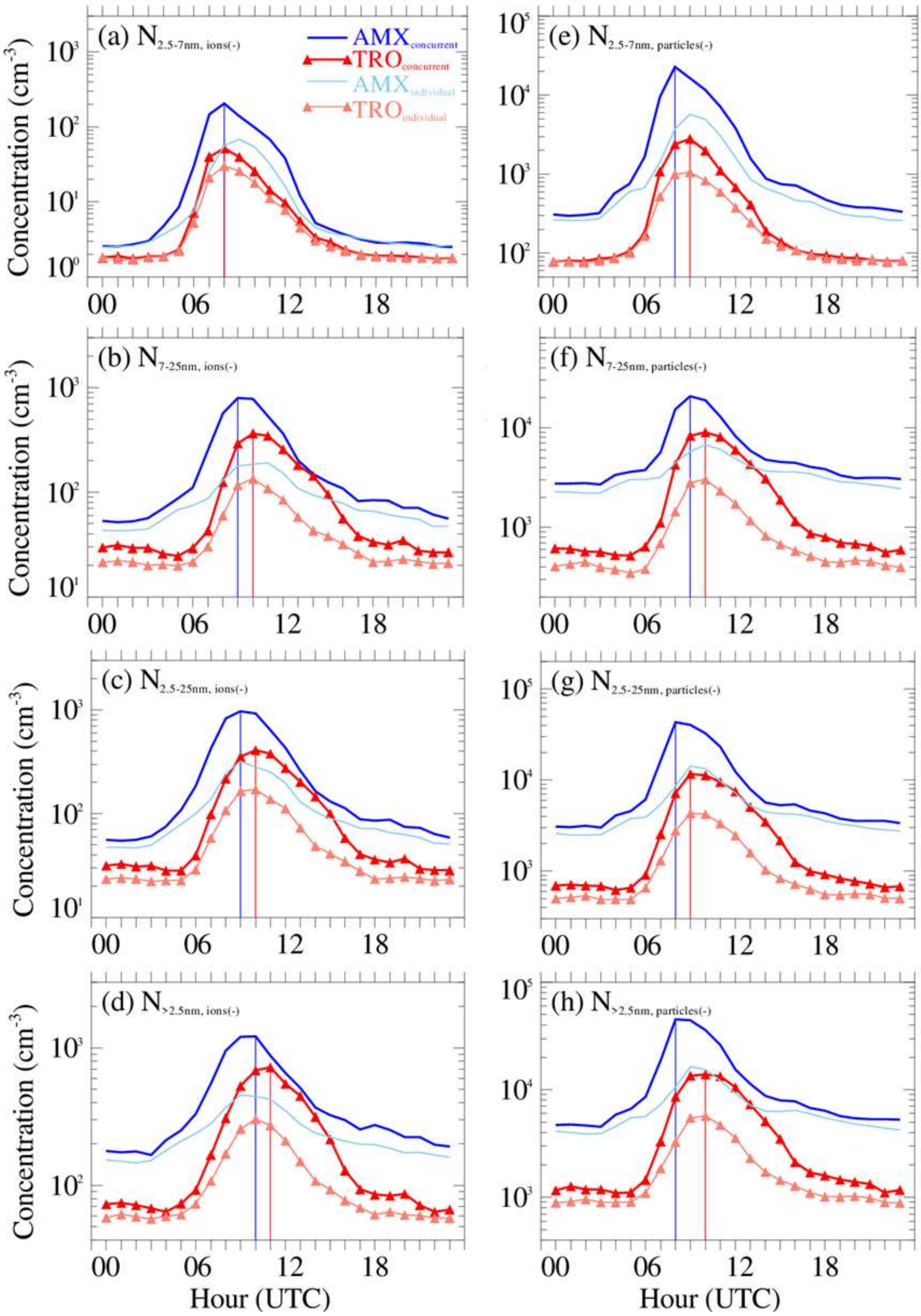


**Figure 4.** Median diurnal variation of negative polarity ion (a-d) and particle (e-h) size-segregated (2.5 - 7 nm, 7 - 25 nm, 2.5 - 25 nm, and >2.5 nm) number concentrations observed on concurrent NPF events at AMX (dark blue thick line) and TRO (dark red thick line). The

light blue and light red lines are for NPF events observed individually at AMX and TRO, respectively. The blue and red vertical lines indicate the times at which the peak concentrations for concurrent NPF events were observed at AMX and TRO, respectively.

The peak in size-segregated ion and particle number concentrations exhibited a time lag of 1-2 hours for concurrent NPF events at both sites (Fig. 4). Further, the size-segregated ion and particle number concentrations were higher at AMX than at TRO. To substantiate our hypothesis, we first obtained NPF event start-times at both sites. The histogram of NPF event start-times indicates that NPF events at the TRO site were consistently detected with a time lag of 1-2 hours compared to AMX (Fig. 5a). We further calculated the time required for the PBL height to reach the TRO altitude relative to the NPF event start-time at AMX ($dT_{PBLevolution}$) and the time lag between peak number concentrations of negative polarity particles >2.5 nm ($dT_{PeakConc., N>2.5 nm, particles(-)}$) for observed concurrent NPF events. Out of 69 concurrent event days, PBL height data was screened out for 24 days (as explained in section 2.3), leaving 45 data points. The average time lags based on particles and PBL measurements are 1.57 hours (~94 minutes) and 1.73 hours (~104 minutes), respectively (Fig. 5b). The mode diameter of negative polarity particles was also larger at TRO than at AMX. At 7:00 UTC, the negative polarity ion (particle) mode diameters at AMX and TRO were about 13.6 nm (7.8 nm) and 15.5 nm (15.7 nm), respectively (Figs. 5c, 5d). Considering the time lag of 2 hours between these sites, the negative polarity particle growth rate is estimated to be ~3.9 nm $hr^{-1}$. The mode diameter of positive polarity particles also showed similar behaviour (Fig. S5a, S5b). During the concurrent NPF event days, the calculated size-segregated growth rates varied from 0.1 to 3.64 nm $hr^{-1}$ (3-7 nm) and 0.18 to 6.08 nm $hr^{-1}$ (7-25 nm) with a mean and standard deviation of 1.53±0.98 nm $hr^{-1}$ and 2.35±1.16 nm $hr^{-1}$, respectively, at AMX while they varied from 0.12 to 2.91 nm $hr^{-1}$ (3-7 nm) and 0.4 to 8.7 nm $hr^{-1}$ (7 – 25 nm) with a mean and standard deviation of 1.49±0.71 nm $hr^{-1}$ and 3.68±2.22 nm $hr^{-1}$, respectively, at TRO. The growth rates of smaller particles (3-7 nm) were similar while the growth rates of larger particles (7-25 nm) were higher at TRO indicating that the particles grew rapidly during upward airmass transport from AMX to TRO due to PBL evolution (see section 3.3, Fig. 7), possibly by valley winds or vertical mixing, on concurrent event days. The size-segregated particle growth rates for positive polarity also showed similar behaviour (Fig. S5c and S5d). The lower number concentrations of nucleation mode particles at TRO than at AMX (Fig. 4) can facilitate more availability of vapour for rapid growth at TRO. Therefore, we next examine PBL evolution and its influence on the TRO mountain site.

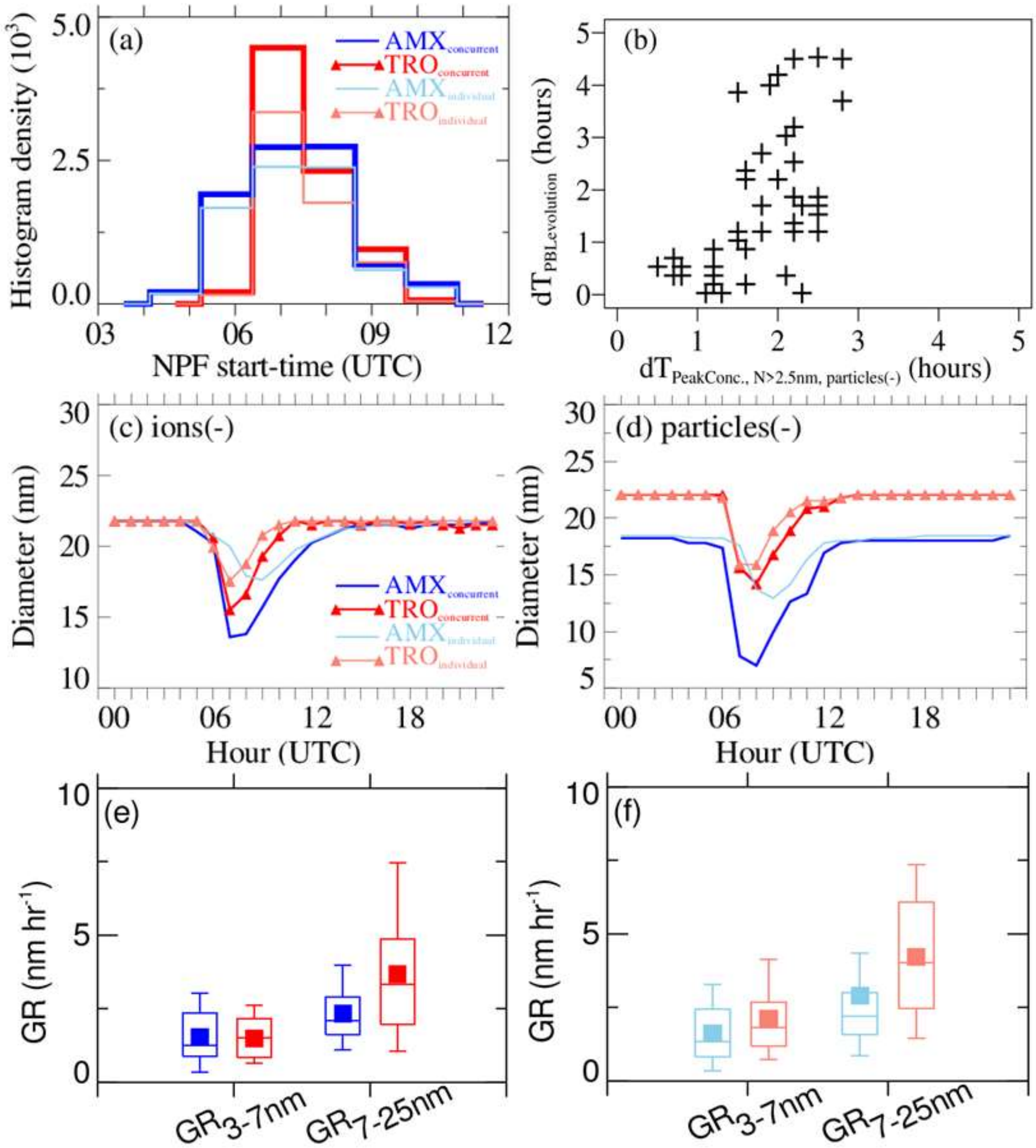


**Figure 5.** (a) Histogram density of NPF events start-time for the observed concurrent NPF events at AMX (dark blue) and TRO (dark red). The light blue and light red coloured lines indicate NPF events observed individually at AMX and TRO, respectively. (b) scatter plot of the time lag between peak number concentrations of negative polarity particles >2.5 nm ($dT_{PeakConc., N>2.5 nm, particles(-)}$) and the time needed for PBL to reach TRO altitude relative to the NPF start-time at AMX ($dT_{PBLevolution}$). Median diurnal variation of negative polarity (c) ion and (d) particle mode diameter. The box-whisker plot of size-segregated particle growth rates for negative polarity for the observed (e) concurrent NPF events and (f) individual NPF events. The filled square indicates the mean, the horizontal line indicates the median, the bottom and

top of the box indicate the 25th and 75th percentiles and the bottom and top of the whisker indicate the 10th and 90th percentiles.

### 3.3 Examining PBL evolution and its influence on the TRO site

The vertical evolution of the PBL significantly influences meteorological and environmental factors, such as near-surface pollutant concentrations, wind velocity, and turbulent exchange of momentum, heat, and moisture (Stull, 1988). The most accurate and common measurements of thermodynamic profiles are achieved using radiosondes, but the temporal resolution is too sparse to detect the evolution of the diurnal structure of PBL. Ground-based remote sensing techniques fill this gap, providing high temporal resolution information, such as sound detection and ranging (SODAR), radio acoustic sounding system (RASS), and light detecting and ranging (LiDAR) (Kotthaus et al., 2023). Here, we used ceilometer measurements from a lower-altitude site (AMX) along with WVMR, passive tracers of PBL dynamics, from both sites to examine the diurnal evolution of the PBL and assess its impact on the mountain site (TRO). Figure 6 shows the monthly median diurnal variation of WVMR at both sites, PBLH at AMX, and the estimates for the influence of the PBL evolution on the TRO site. The monthly median diurnal variation of WVMR illustrates the probable mixing of air between the lower-altitude AMX site and the mountain TRO site (e.g. up-valley wind or vertical mixing) except during late winter and early spring (Fig. 6a, b). Concurrently, the WVMRs at the TRO site were consistently lower than the threshold of 5.25 g/kg during late winter and early spring, suggesting that the site is primarily influenced by free tropospheric (FT) air (Fig. 6b). The pattern was reinforced by the analysis of PBLH, exhibiting similar seasonal cycle. The monthly median PBLH was found to be lower than the altitude of the TRO site during late winter and early spring, and higher for the remainder of the year. We further calculated the occurrence frequency of PBLH at AMX exceeding the altitude of the TRO site (1287 m above AMX) and WVMR at TRO exceeding a threshold value of 5.25 g/kg. The occurrence frequencies demonstrate the observed seasonal and diurnal patterns in PBL influence on the TRO site (Figs. 6d, 6e). This suggests that the TRO site is periodically influenced by the PBL evolution during later winter and early spring, whereas it is primarily within the PBL for the remainder of the year. Lastly, Figure 6f shows the monthly fraction of days when the TRO site is influenced by the evolution of PBL. The TRO site is within the PBL on approximately 25% of days during late winter and early spring, increasing to >80% for the remainder of the year. The concurrent patterns observed in these tracers (PBLH and WVMR) suggest that the TRO site is impacted by the transport of polluted air from lower-elevation regions, possibly through vertical mixing or up-valley wind. Previous studies have demonstrated that up-valley winds can facilitate the upward movement of aerosol precursors, which can rapidly form a large number of new aerosol particles, and pre-existing particles from lower-altitude regions to mountain measurement sites, particularly within an elevated PBL (Bianchi et al., 2021; Hooda et al., 2018; Sebastian et al., 2021; Cusack et al., 2013).

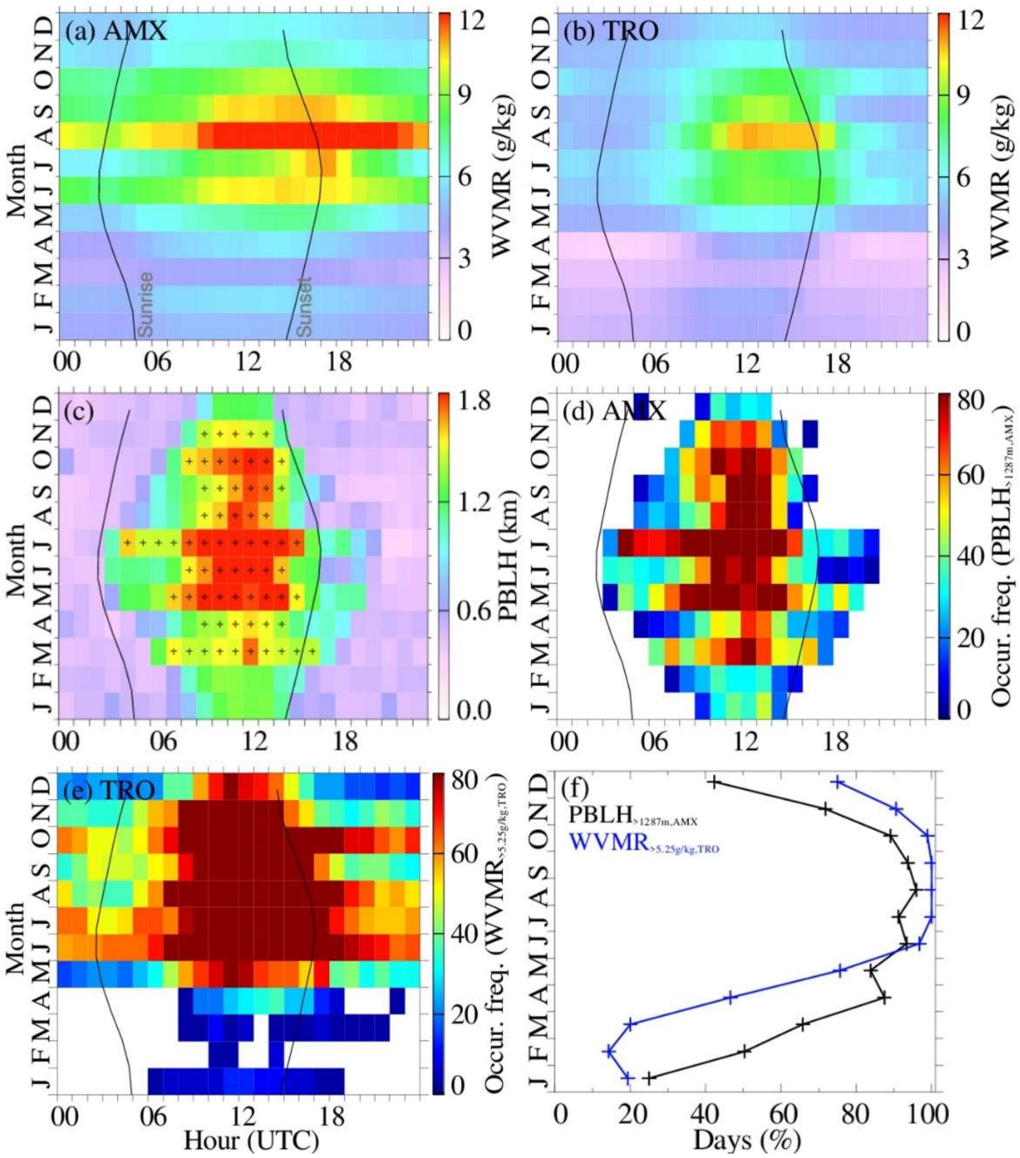


**Figure 6**. Monthly median diurnal variation of WVMR at (a) AMX, (b) TRO, and (c) PBLH at AMX. The pixels with a plus sign in (c) indicate the times of the day when PBLH is higher than the altitude of the TRO site (1287 m above the AMX site). (d) monthly median diurnal variation of the occurrence frequency of PBLH higher than the altitude of the TRO site, (e) monthly median diurnal variation of the occurrence frequency of WVMR > 5.25 g/kg at TRO, indicative of the PBL evolution up to the altitude of the TRO site, and (f) monthly fraction of

days the TRO site is influenced by the evolution of PBL as illustrated by PBLH higher than the altitude of the TRO site and WVMR > 5.25 g/kg at TRO. The grey thin lines in (a)-(e) indicate UTC sunrise and sunset times.

To further substantiate our hypothesis, we examined the air mass history at the TRO site during observed concurrent NPF event days. Figure 7 shows the vertical cross-section of the fraction of air mass backward trajectories arriving at the TRO for observed concurrent NPF events. A large fraction of air masses had spent considerable time within the PBL before ascending to the altitude of the TRO site during concurrent NPF events at TRO. The monthly averaged airmass backward trajectories on concurrent NPF events showed that the free tropospheric air masses descended into the PBL upon entering the Mediterranean Sea, then they travelled along the surface towards the AMX site (Fig. S6) and eventually ascended to the TRO site altitude and above in response to the evolving PBL during the day (Fig. 7). The amplitude of the diurnal pattern of aerosol properties is the highest for the concurrent NPF events (Figs. 4, 5), further substantiating that the TRO site experiences daytime evolution of the PBL, analogous to a previous study demonstrating the daytime PBL influence due to vertical mixing (Collaud Coen et al., 2018). On the other hand, the airmass backward trajectories on individual NPF event days at these sites show distinct air mass history (Fig. S7).

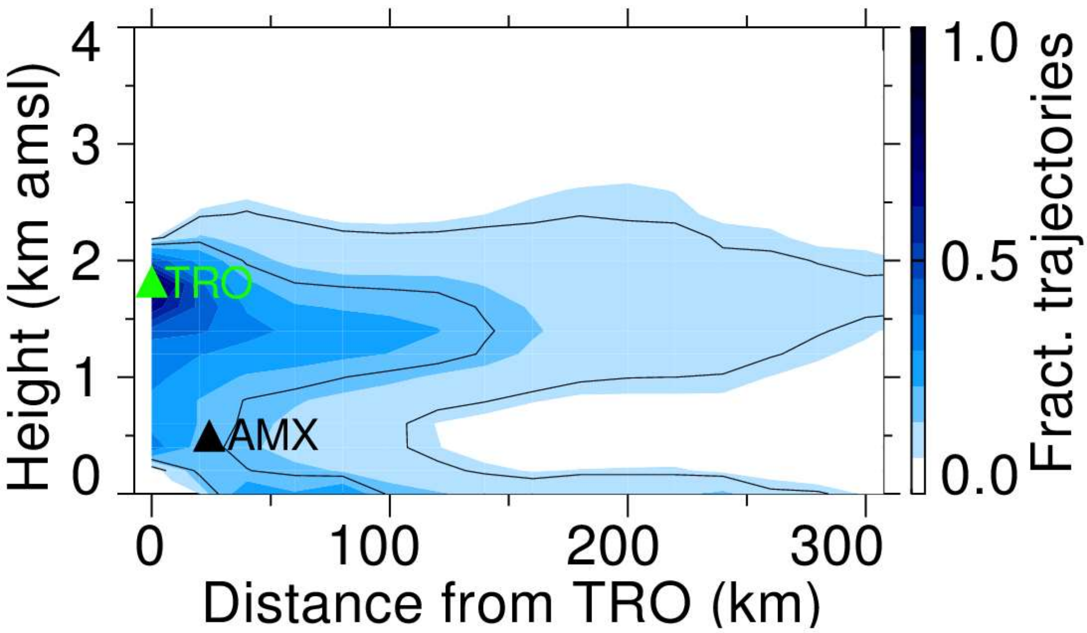

**Figure 7.** Vertical cross-section of the fraction of airmass backward trajectories arriving at the TRO site (6 - 12 UTC) for the observed concurrent NPF events. The green and black upward triangle indicates TRO and AMX elevation above mean sea level, respectively.

## 4. Discussions

The frequency of occurrence of NPF events was comparable between AMX (a lower-altitude rural site) and TRO (a higher-altitude mountain site) in Cyprus, as opposed to the findings of Boulon et al. (2011) in Central France, where NPF events were more frequent at a mountain site (the Puy de Dôme station, 1465 m a.m.s.l.) than at a nearby rural lower-altitude site (the Opme station, 660 m a.m.s.l., about 12 km southeast of the Puy de Dôme station). The follow-up study by Farah et al. (2018) used PBL tracers, such as particle size distribution and black carbon concentrations, to distinguish between free-tropospheric and PBL air masses at Puy de Dôme. They found that the Puy de Dôme station is within the PBL 50% of the time during the winter and up to 97% during the summer. Since most mountain sites are typically within the PBL during the day, it is important to investigate whether the evolving PBL influences these mountain sites when NPF occurs. The AMX and TRO sites are also located close to each other, approximately 20 km apart, yet we observed similar NPF frequencies at both (Fig. 3a). About half of the NPF events occurred simultaneously at both sites (Fig. 3d), particularly when the air masses originated from the northwest to northeast corridor relative to the TRO site. At measurement sites situated above 1000 m a.s.l., higher condensation sink tend to favour NPF, likely due to the presence of precursor gases needed to initiate nucleation and early growth (Sellegri et al., 2019), which is thought to be linked to vertically elevated precursor gases that promote particle formation and growth (in our case, $SO_2$ concentrations were higher during NPF events than non-events at TRO, Fig. S3c). Measurements from a remote background site in the western Himalayas also indicated that NPF was favoured under the influence of anthropogenic plumes with a higher condensation sink indicative of the precursor- and aerosol-laden air (Sebastian et al., 2021). Measurements from a remote mountain site (Mount Heng, Huan Province) in South China further demonstrated that NPF events are favoured during heavy dust episodes mixed with anthropogenic pollution (Nie et al., 2014). All of these studies suggest that the balance between precursor vapours and pre-existing particles in homogenously mixed air masses determines when NPF is favoured in the atmosphere (Kanawade et al., 2021; Hyvärinen et al., 2010).

A previous study demonstrated that the 30-minute time lag between black carbon concentrations and the cluster ion mode suggests that nucleation processes may be initiated at the interface between the PBL and the free troposphere (Sellegri et al., 2019). However, the 1–2 hour time lag and the higher magnitude of aerosol properties at the AMX site compared to TRO (Figs. 4, S2, S3c, and S4a) suggest nucleation processes likely occurred within the well-mixed PBL. Airborne observations of sub-3 nm particles over boreal forests showed that the total particle number concentrations (>1.5 nm) are the highest near the ground in the morning, and the aerosol population is well mixed within evolving PBL later in the day (Leino et al., 2019). Crumeyrolle et al. (2010) also showed that nucleation occurs within the boundary layer, with the vertical extension of NPF events not exceeding the boundary layer's top. This can be explained by turbulent mixing leading to local supersaturation of condensable vapours and the dispersion of pre-existing particles, which in turn could enhance the nucleation process within the well-mixed PBL. Even at higher-altitude sites like the Jungfraujoch station (3580 m a.m.s.l.), previous studies have shown that NPF events can occur in free tropospheric air masses, provided these air masses are in contact with the PBL before reaching to higher-altitude site (Bianchi et al., 2016; Tröstl et al., 2016b). Carnerero et al. (2018) also showed that ultrafine particles are formed within the mixed layer, and as this layer expands, these particles are subsequently detected at higher altitudes within the PBL. On the contrary, Platis et al. (2016) provided observational evidence of the inversion layer facilitating thermodynamic conditions for NPF at elevated altitudes within the PBL, and subsequently, these particles moved toward the ground. Several other studies also showed that NPF events preferentially take place in the free troposphere (Clarke and Kapustin, 2002; Hamburger et al., 2011; Rose et al., 2015), or at the interface between the PBL and the free troposphere (Wehner et al., 2015).

Nonetheless, only about 50% of NPF events occurred concurrently at both sites when air masses originated from the northwest to northeast corridor (with AMX located north-northeast of TRO). Figure S7 illustrates the monthly-averaged, two-day backward air mass trajectories as a function of altitude for NPF events at AMX and TRO. Despite the proximity of these sites (~20 km), NPF events often occur in distinct air masses (Fig. S7). At TRO, the remaining events were linked to free-tropospheric air masses or the PBL under similar conditions, with air masses arriving from the southwest to the southeast corridor. Air mass history together with the intense solar radiation, the intricate mixture of both natural and anthropogenic emissions from continental and marine origins, the presence of local breeze systems (mountain, valley, sea, and land) and elevated dust layers over the region poses a significant challenge in understanding the drivers behind the frequent NPF events observed in Cyprus and, therefore adds complexity to the PBL–NPF relationship.

## 5. Conclusions

This work presents the concurrent observations of ion and particle size distributions from a rural background lower-altitude site (Agia Marina Xyliatou, 532 m a.m.s.l.) and a higher-altitude background mountain site (Troodos, 1819 m a.m.s.l.) in Cyprus for the year 2022. We investigated the influence of boundary layer evolution on the NPF occurrence at a background mountain site, TRO. We found that the NPF event frequency was comparable between AMX (129 days out of 214 valid observation days, 60%) and TRO (121 days out of 224 valid observation days, 54%). Out of these, NPF events occurred concurrently at both sites on 69 days. Typical NPF events at AMX and TRO exhibited distinct patterns, with AMX showing a significantly longer-lasting banana-shaped distribution below 10 nm diameter compared to TRO, suggesting differences in the supply of precursor vapours. During concurrent NPF events, the smaller mode diameter at the AMX site implies that nucleation processes occur nearby, while the particles have grown larger before they are detected at TRO.

By combining measurements from the higher-altitude TRO site with those from the lower-altitude AMX site, we were able to investigate the influence of evolving PBL on the nucleation processes in this remote mountainous region. For this, we used ceilometer measurements from AMX along with WVMR, passive tracers of PBL dynamics, from both sites to examine the diurnal evolution of the PBL. Our analyses indicated that the TRO site is within the PBL on approximately 25% of days during late winter and early spring, increasing to >80% of days for the remainder of the year. We used 69 days of concurrent NPF events days and compared them with individual NPF events at both sites. The peak in size-segregated ion and particle number concentrations occurred at the same time of day for individual NPF events at both sites. In contrast, for concurrent NPF events, the peak was observed at the lower-altitude site first, followed by a 1-2 hour time delay at the mountain site, TRO, suggesting the vertical extent of the nucleation process within the PBL. In these cases, NPF events at TRO are linked to the evolving PBL since the nucleation is detected at TRO when the PBL extends over the altitude of the TRO site. This was substantiated by a 1-hour delay in the NPF events start-time and a relatively larger particle mode diameter at TRO. This suggests that the transport of precursor vapour-laden air from lower-altitude regions, likely driven by vertical mixing or up-valley winds, might play a significant role in the aerosol formation process in the higher-altitude site.

The airmass history for concurrent NPF events revealed that a significant fraction of the airmass trajectories had previously been in contact with the PBL before reaching the TRO site. This suggests the vertical extent of NPF processes within the evolving PBL, though this requires further critical investigation. The influence of evolving PBL at a mountain site in this study reflects similarities with those reported in earlier studies, showing observed NPF events at a higher-altitude site, whether within or above PBL, have always been linked with the PBL (Bianchi et al., 2016; Carnerero et al., 2018; Sebastian et al., 2021; Sellegri et al., 2019; Bianchi et al., 2021; Hooda et al., 2018), except those observed in the middle-upper troposphere and stratosphere or convective cloud outflows.

Despite significant progress in regional and global climate models enhanced with process-based parameterisations derived from controlled laboratory experiments, ambient measurements, and space-borne observations, a comprehensive understanding of the climate system remains elusive. The aerosol-cloud interaction is one of the largest sources of uncertainty in the climate system, primarily due to ambiguity in CCN production, which arises from uncertainties in both primary emissions and airborne secondary production (IPCC, 2023). Furthermore, the uneven geographical distribution and spatial heterogeneity of measurement networks, coupled with asynchronous monitoring and inconsistent data collection methods for various atmospheric variables hinder the ability to constrain model assimilation and validation. Thus, the process-level understanding of atmospheric processes, their interactions and feedback from them, such as the intricate mixture of primary emissions and airborne production of aerosols, is crucial for advancing future climate predictions, particularly the EMME region which has been recognised as a global climate change hotspot with high vulnerability to climate change impacts.

***Data availability.***

In-situ measurements of ion and particle size distributions, meteorological parameters and gases can be accessed at Zenodo (DOI: https://doi.org/10.5281/zenodo.13970203). The ceilometer data can be viewed at https://e-profile.eu/ (last accessed 22 October 2024). ERA5 boundary layer height data is publicly available from https://cds.climate.copernicus.eu/datasets/reanalysis-era5-single-levels (last accessed 22 October 2024). AERONET aerosol optical depth and Ångstrom exponent data are available publicly to download from https://aeronet.gsfc.nasa.gov/ (last accessed 22 October 2024)

***Author contributions***

FM, JS, MK, KL and TJ designed the experiments and ND, AP, RB, and MP carried them out. ND, VPK and AP analysed the data. ND, VPK and TJ prepared the manuscript with contributions from all co-authors.

***Competing interests.***

At least one of the (co-)authors is a member of the editorial board of Aerosol Research. The authors declare that they have no conflict of interest.

***Acknowledgements.***

This work has been supported by the European Union's Horizon 2020 Research and Innovation Programme under grant agreement No. 856612 and the Cyprus Government. TJ acknowledges the funding support by the European Union ERC-2022-STGERC-BAE-Project: 101076311. Views and opinions expressed are however those of the author(s) only and do not necessarily reflect those of the European Union or the European Research Council Executive Agency. Neither the European Union nor the granting authority can be held responsible for them. The authors thank the University of Helsinki, INAR/Physics for support and instrumentation, and ACTRIS Cluster Calibration Center for calibration services. The authors also thank the technical support team; Nikoleta Lekaki, Moreno Parolin, and Rafail Konatzii for the technical support in maintaining field stations. The authors thank all the past and present personnel who contributed to the field measurements within the EMME project. The authors thank the anonymous reviewers for their valuable suggestions and comments.

**References**

Aktypis, A., Kaltsonoudis, C., Skyllakou, K., Matrali, A., Vasilakopoulou, C. N., Florou, K., and Pandis, S. N.: Infrequent new particle formation in a coastal Mediterranean city during the summer, Atmos. Environ., 302, 119732, https://doi.org/10.1016/j.atmosenv.2023.119732, 2023.

Aktypis, A., Kaltsonoudis, C., Patoulias, D., Kalkavouras, P., Matrali, A., Vasilakopoulou, C. N., Kostenidou, E., Florou, K., Kalivitis, N., Bougiatioti, A., Eleftheriadis, K., Vratolis, S., Gini, M. I., Kouras, A., Samara, C., Lazaridis, M., Chatoutsidou, S. E., Mihalopoulos, N., and Pandis, S. N.: Significant spatial gradients in new particle formation frequency in Greece during summer, Atmos. Chem. Phys., 24, 65-84, https://doi.org/10.5194/acp-24-65-2024, 2024.

Baalbaki, R., Pikridas, M., Jokinen, T., Laurila, T., Dada, L., Bezantakos, S., Ahonen, L., Neitola, K., Maisser, A., Bimenyimana, E., Christodoulou, A., Unga, F., Savvides, C., Lehtipalo, K., Kangasluoma, J., Biskos, G., Petäjä, T., Kerminen, V. M., Sciare, J., and Kulmala, M.: Towards understanding the characteristics of new particle formation in the Eastern Mediterranean, Atmos. Chem. Phys., 21, 9223-9251, https://doi.org/10.5194/acp-21-9223-2021, 2021.

Bianchi, F., Junninen, H., Bigi, A., Sinclair, V. A., Dada, L., Hoyle, C. R., Zha, Q., Yao, L., Ahonen, L. R., Bonasoni, P., Buenrostro Mazon, S., Hutterli, M., Laj, P., Lehtipalo, K., Kangasluoma, J., Kerminen, V. M., Kontkanen, J., Marinoni, A., Mirme, S., Molteni, U., Petäjä, T., Riva, M., Rose, C., Sellegri, K., Yan, C., Worsnop, D. R., Kulmala, M., Baltensperger, U., and Dommen, J.: Biogenic particles formed in the Himalaya as an important source of free tropospheric aerosols, Nat. Geosci., 14, 4-9, https://doi.org/10.1038/s41561-020-00661-5, 2021.

Bianchi, F., Tröstl, J., Junninen, H., Frege, C., Henne, S., Hoyle, C. R., Molteni, U., Herrmann, E., Adamov, A., Bukowiecki, N., Chen, X., Duplissy, J., Gysel, M., Hutterli, M., Kangasluoma, J., Kontkanen, J., Kürten, A., Manninen, H. E., Münch, S., Peräkylä, O., Petäjä, T., Rondo, L., Williamson, C., Weingartner, E., Curtius, J., Worsnop, D. R., Kulmala, M., Dommen, J., and Baltensperger, U.: New particle formation in the free troposphere: A question of chemistry and timing, Science, 352, 1109-1112, https://doi.org/10.1126/science.aad5456, 2016.

Bimenyimana, E., Pikridas, M., Oikonomou, K., Iakovides, M., Christodoulou, A., Sciare, J., and Mihalopoulos, N.: Fine aerosol sources at an urban background site in the Eastern Mediterranean (Nicosia; Cyprus): Insights from offline versus online source apportionment comparison for carbonaceous aerosols, Sci. Total Environ., 893, 164741, https://doi.org/10.1016/j.scitotenv.2023.164741, 2023.

Boulon, J., Sellegri, K., Hervo, M., Picard, D., Pichon, J. M., Fréville, P., and Laj, P.: Investigation of nucleation events vertical extent: a long term study at two different altitude sites, Atmos. Chem. Phys., 11, 5625-5639, https://doi.org/10.5194/acp-11-5625-2011, 2011.

Brilke, S., Fölker, N., Müller, T., Kandler, K., Gong, X., Peischl, J., Weinzierl, B., and Winkler, P. M.: New particle formation and sub-10 nm size distribution measurements during the A-LIFE field experiment in Paphos, Cyprus, Atmos. Chem. Phys., 20, 5645-5656, https://doi.org/10.5194/acp-20-5645-2020, 2020.

Buck, A. L.: New Equations for Computing Vapor Pressure and Enhancement Factor, *J. Appl. Meteorol. Climatol.*, 20, 1527-1532, https://doi.org/10.1175/1520-0450(1981)020<1527:NEFCVP>2.0.CO;2, 1981.

Buenrostro Mazon, S., Riipinen, I., Schultz, D. M., Valtanen, M., Dal Maso, M., Sogacheva, L., Junninen, H., Nieminen, T., Kerminen, V.-M., and Kulmala, M.: Classifying previously undefined days from eleven years of aerosol-particle-size distribution data from the SMEAR II station, Hyytiälä, Finland, Atmos. Chem. Phys., 9, 667-676, https://doi.org/10.5194/acp-9-667-2009, 2009.

Carnerero, C., Pérez, N., Reche, C., Ealo, M., Titos, G., Lee, H. K., Eun, H. R., Park, Y. H., Dada, L., Paasonen, P., Kerminen, V. M., Mantilla, E., Escudero, M., Gómez-Moreno, F. J., Alonso-Blanco, E., Coz, E., Saiz-Lopez, A., Temime-Roussel, B., Marchand, N., Beddows, D. C. S., Harrison, R. M., Petäjä, T., Kulmala, M., Ahn, K. H., Alastuey, A., and Querol, X.:

Vertical and horizontal distribution of regional new particle formation events in Madrid, Atmos. Chem. Phys., 18, 16601-16618, https://doi.org/10.5194/acp-18-16601-2018, 2018.

Clarke, A. D. and Kapustin, V. N.: A Pacific Aerosol Survey. Part I: A Decade of Data on Particle Production, Transport, Evolution, and Mixing in the Troposphere J. Atmos. Sci., 59, 363-382, https://doi.org/10.1175/1520-0469(2002)059<0363:APASPI>2.0.CO;2, 2002.

Clarke, A. D., Varner, J. L., Eisele, F., Mauldin, R. L., Tanner, D., and Litchy, M.: Particle production in the remote marine atmosphere: Cloud outflow and subsidence during ACE 1, J. Geophys. Res.103, 16397-16409, https://doi.org/10.1029/97JD02987, 1998.

Collaud Coen, M., Andrews, E., Aliaga, D., Andrade, M., Angelov, H., Bukowiecki, N., Ealo, M., Fialho, P., Flentje, H., Hallar, A. G., Hooda, R., Kalapov, I., Krejci, R., Lin, N. H., Marinoni, A., Ming, J., Nguyen, N. A., Pandolfi, M., Pont, V., Ries, L., Rodríguez, S., Schauer, G., Sellegri, K., Sharma, S., Sun, J., Tunved, P., Velasquez, P., and Ruffieux, D.: Identification of topographic features influencing aerosol observations at high altitude stations, Atmos. Chem. Phys., 18, 12289-12313, https://doi.org/10.5194/acp-18-12289-2018, 2018.

Crumeyrolle, S., Manninen, H. E., Sellegri, K., Roberts, G., Gomes, L., Kulmala, M., Weigel, R., Laj, P., and Schwarzenboeck, A.: New particle formation events measured on board the ATR-42 aircraft during the EUCAARI campaign, Atmos. Chem. Phys., 10, 6721-6735, https://doi.org/10.5194/acp-10-6721-2010, 2010.

Cusack, M., Alastuey, A., and Querol, X.: Case studies of new particle formation and evaporation processes in the western Mediterranean regional background, Atmos. Environ., 81, 651-659, https://doi.org/10.1016/j.atmosenv.2013.09.025, 2013.

Dal Maso, M., Kulmala, M., Riipinen, I., Wagner, R., Hussein, T., Aalto, P. P., and Lehtinen, K. E. J.: Formation and growth of fresh atmospheric aerosols: eight years of aerosol size distribution data from SMEAR II, Hyytiälä, Finland, Boreal Env. Res., 10, 323-336, ISSN 1239-6095, 2005.

Debevec, C., Sauvage, S., Gros, V., Sellegri, K., Sciare, J., Pikridas, M., Stavroulas, I., Leonardis, T., Gaudion, V., Depelchin, L., Fronval, I., Sarda-Esteve, R., Baisnée, D., Bonsang, B., Savvides, C., Vrekoussis, M., and Locoge, N.: Driving parameters of biogenic volatile organic compounds and consequences on new particle formation observed at an eastern Mediterranean background site, Atmos. Chem. Phys., 18, 14297-14325, https://doi.org/10.5194/acp-18-14297-2018, 2018.

Dinoi, A., Gulli, D., Weinhold, K., Ammoscato, I., Calidonna, C. R., Wiedensohler, A., and Contini, D.: Characterization of ultrafine particles and the occurrence of new particle formation events in an urban and coastal site of the Mediterranean area, Atmos. Chem. Phys., 23, 2167-2181, https://doi.org/10.5194/acp-23-2167-2023, 2023.

Draxler, R. R. and Rolph, G. D.: HYSPLIT (HYbrid Single-Particle Lagrangian Integrated Trajectory) Model Access via NOAA ARL READY Website. NOAA Air Resources Laboratory, Silver Spring.http://ready.arl.noaa.gov/HYSPLIT.php, 2010.

Emeis, S., Jahn, C., Münkel, C., Münsterer, C., and Schäfer, K.: Multiple atmospheric layering and mixing-layer height in the Inn valley observed by remote sensing, Meteorol. Z., 16, 415-424, https://doi.org/10.1127/0941?2948/2007/0203, 2007.

Farah, A., Freney, E., Chauvigné, A., Baray, J.-L., Rose, C., Picard, D., Colomb, A., Hadad, D., Abboud, M., Farah, W., and Sellegri, K.: Seasonal variation of aerosol size distribution data at the Puy de Dôme station with emphasis on the boundary layer/free troposphere segregation, Atmosphere, 9, 244, https://doi.org/10.3390/atmos9070244, 2018.

Gong, X., Wex, H., Müller, T., Wiedensohler, A., Höhler, K., Kandler, K., Ma, N., Dietel, B., Schiebel, T., Möhler, O., and Stratmann, F.: Characterization of aerosol properties at Cyprus, focusing on cloud condensation nuclei and ice-nucleating particles, Atmos. Chem. Phys., 19, 10883-10900, 10.5194/acp-19-10883-2019, 2019.

Gordon, H., Kirkby, J., Baltensperger, U., Bianchi, F., Breitenlechner, M., Curtius, J., Dias, A., Dommen, J., Donahue, N. M., Dunne, E. M., Duplissy, J., Ehrhart, S., Flagan, R. C., Frege, C., Fuchs, C., Hansel, A., Hoyle, C. R., Kulmala, M., Kürten, A., Lehtipalo, K., Makhmutov, V., Molteni, U., Rissanen, M. P., Stozkhov, Y., Tröstl, J., Tsagkogeorgas, G., Wagner, R., Williamson, C., Wimmer, D., Winkler, P. M., Yan, C., and Carslaw, K. S.: Causes and importance of new particle formation in the present-day and preindustrial atmospheres, J. Geophys. Res., 122, 8739-8760, https://doi.org/10.1002/2017jd026844, 2017.

Gormley, P. G. and Kennedy, M.: Diffusion from a Stream Flowing Through a Cylindrical Tube, Proc. R. Ir. Acad., Sect. A, 52, 163-169, https://www.jstor.org/stable/20488498, 1949.

Hakala, S., Vakkari, V., Lihavainen, H., Hyvärinen, A. P., Neitola, K., Kontkanen, J., Kerminen, V. M., Kulmala, M., Petäjä, T., Hussein, T., Khoder, M. I., Alghamdi, M. A., and Paasonen, P.: Explaining apparent particle shrinkage related to new particle formation events in western Saudi Arabia does not require evaporation, Atmos. Chem. Phys., 23, 9287-9321, https://doi.org/10.5194/acp-23-9287-2023, 2023.

Hakala, S., Alghamdi, M. A., Paasonen, P., Vakkari, V., Khoder, M. I., Neitola, K., Dada, L., Abdelmaksoud, A. S., Al-Jeelani, H., Shabbaj, I. I., Almehmadi, F. M., Sundström, A. M., Lihavainen, H., Kerminen, V. M., Kontkanen, J., Kulmala, M., Hussein, T., and Hyvärinen, A. P.: New particle formation, growth and apparent shrinkage at a rural background site in western Saudi Arabia, Atmos. Chem. Phys., 19, 10537-10555, https://doi.org/10.5194/acp-19-10537-2019, 2019.

Hamburger, T., McMeeking, G., Minikin, A., Birmili, W., Dall'Osto, M., O'Dowd, C., Flentje, H., Henzing, B., Junninen, H., Kristensson, A., de Leeuw, G., Stohl, A., Burkhart, J. F., Coe, H., Krejci, R., and Petzold, A.: Overview of the synoptic and pollution situation over Europe during the EUCAARI-LONGREX field campaign, Atmos. Chem. Phys., 11, 1065-1082, https://doi.org/10.5194/acp-11-1065-2011, 2011.

Hersbach, H., Bell, B., Berrisford, P., Biavati, G., Horányi, A., Muñoz Sabater, J., Nicolas, J., Peubey, C., Radu, R., Rozum, I., Schepers, D., Simmons, A., Soci, C., Dee, D., and Thépaut, J.-N.: ERA5 hourly data on pressure levels from 1940 to present. Copernicus Climate Change Service (C3S) Climate Data Store (CDS), https://doi.org/10.24381/cds.bd0915c6, 2023.

Hersbach, H., Bell, B., Berrisford, P., Hirahara, S., Horányi, A., Muñoz-Sabater, J., Nicolas, J., Peubey, C., Radu, R., Schepers, D., Simmons, A., Soci, C., Abdalla, S., Abellan, X., Balsamo, G., Bechtold, P., Biavati, G., Bidlot, J., Bonavita, M., De Chiara, G., Dahlgren, P., Dee, D., Diamantakis, M., Dragani, R., Flemming, J., Forbes, R., Fuentes, M., Geer, A., Haimberger, L., Healy, S., Hogan, R. J., Hólm, E., Janisková, M., Keeley, S., Laloyaux, P., Lopez, P., Lupu, C., Radnoti, G., de Rosnay, P., Rozum, I., Vamborg, F., Villaume, S., and

Thépaut, J.-N.: The ERA5 global reanalysis, Q. J. R. Meteorol. Soc., 146, 1999-2049, https://doi.org/10.1002/qj.3803, 2020.

Hirsikko, A., Bergman, T., Laakso, L., Dal Maso, M., Riipinen, I., Hõrrak, U., and Kulmala, M.: Identification and classification of the formation of intermediate ions measured in boreal forest, Atmos. Chem. Phys., 7, 201-210, https://doi.org/10.5194/acp-7-201-2007, 2007.

Hirsikko, A., Vakkari, V., Tiitta, P., Manninen, H. E., Gagné, S., Laakso, H., Kulmala, M., Mirme, A., Mirme, S., Mabaso, D., Beukes, J. P., and Laakso, L.: Characterisation of sub-micron particle number concentrations and formation events in the western Bushveld Igneous Complex, South Africa, Atmos. Chem. Phys., 12, 3951-3967, https://doi.org/10.5194/acp-12-3951-2012, 2012.

Hooda, R. K., Kivekäs, N., O'Connor, E. J., Collaud Coen, M., Pietikäinen, J.-P., Vakkari, V., Backman, J., Henriksson, S. V., Asmi, E., Komppula, M., Korhonen, H., Hyvärinen, A.-P., and Lihavainen, H.: Driving Factors of Aerosol Properties Over the Foothills of Central Himalayas Based on 8.5 Years Continuous Measurements, J. Geophys. Res., 123, 13,421-413,442, https://doi.org/10.1029/2018jd029744, 2018.

Hussein, T., Atashi, N., Sogacheva, L., Hakala, S., Dada, L., Petäjä, T., and Kulmala, M.: Characterization of Urban New Particle Formation in Amman—Jordan, Atmosphere, 11, 79, https://doi.org/10.3390/atmos11010079 2020.

Hyvärinen, A. P., Lihavainen, H., Komppula, M., Panwar, T. S., Sharma, V. P., Hooda, R. K., and Viisanen, Y.: Aerosol measurements at the Gual Pahari EUCAARI station: preliminary results from in-situ measurements, Atmos. Chem. Phys., 10, 7241-7252, https://doi.org/10.5194/acp-10-7241-2010, 2010.

IPCC: Climate Change 2023: Synthesis Report. Contribution of Working Groups I, II and III to the Sixth Assessment Report of the Intergovernmental Panel on Climate Change [Core Writing Team, H. Lee and J. Romero (eds.)]. IPCC, Geneva, Switzerland, 184 pp., http://doi.org/10.59327/IPCC/AR6-9789291691647, 2023.

Kalivitis, N., Kerminen, V. M., Kouvarakis, G., Stavroulas, I., Tzitzikalaki, E., Kalkavouras, P., Daskalakis, N., Myriokefalitakis, S., Bougiatioti, A., Manninen, H. E., Roldin, P., Petäjä, T., Boy, M., Kulmala, M., Kanakidou, M., and Mihalopoulos, N.: Formation and growth of atmospheric nanoparticles in the eastern Mediterranean: results from long-term measurements and process simulations, Atmos. Chem. Phys., 19, 2671-2686, https://doi.org/10.5194/acp-19-2671-2019, 2019.

Kalkavouras, P., Bougiatioti, A., Hussein, T., Kalivitis, N., Stavroulas, I., Michalopoulos, P., and Mihalopoulos, N.: Regional New Particle Formation over the Eastern Mediterranean and Middle East, Atmosphere, 12, https://doi.org/10.3390/atmos12010013, 2021.

Kalkavouras, P., Bougiatioti, A., Kalivitis, N., Stavroulas, I., Tombrou, M., Nenes, A., and Mihalopoulos, N.: Regional new particle formation as modulators of cloud condensation nuclei and cloud droplet number in the eastern Mediterranean, Atmos. Chem. Phys., 19, 6185-6203, https://doi.org/10.5194/acp-19-6185-2019, 2019.

Kalkavouras, P., Bougiatioti, A., Grivas, G., Stavroulas, I., Kalivitis, N., Liakakou, E., Gerasopoulos, E., Pilinis, C., and Mihalopoulos, N.: On the regional aspects of new particle formation in the Eastern Mediterranean: A comparative study between a background and an urban site based on long term observations, Atmos. Res., 239, 104911, https://doi.org/10.1016/j.atmosres.2020.104911, 2020.

Kanawade, V. P., Sebastian, M., Hooda, R. K., and Hyvärinen, A. P.: Atmospheric new particle formation in India: Current understanding, knowledge gaps and future directions, Atmos. Environ., 270, 118894, https://doi.org/10.1016/j.atmosenv.2021.118894, 2021.

Kanawade, V. P., Tripathi, S. N., Siingh, D., Gautam, A. S., Srivastava, A. K., Kamra, A. K., Soni, V. K., and Sethi, V.: Observations of new particle formation at two distinct Indian subcontinental urban locations, Atmos. Environ., 96, 370-379, http://dx.doi.org/10.1016/j.atmosenv.2014.08.001, 2014.

Kerminen, V. M., Chen, X., Vakkari, V., Petäjä, T., Kulmala, M., and Bianchi, F.: Atmospheric new particle formation and growth: review of field observations, Environ. Res. Lett., 13, 103003, https://doi.org/10.1088/1748-9326/aadf3c, 2018.

Kerminen, V. M., Paramonov, M., Anttila, T., Riipinen, I., Fountoukis, C., Korhonen, H., Asmi, E., Laakso, L., Lihavainen, H., Swietlicki, E., Svenningsson, B., Asmi, A., Pandis, S. N., Kulmala, M., and Petäjä, T.: Cloud condensation nuclei production associated with atmospheric nucleation: a synthesis based on existing literature and new results, Atmos. Chem. Phys., 12, 12037-12059, https://doi.org/10.5194/acp-12-12037-2012, 2012.

Kotthaus, S., Bravo-Aranda, J. A., Collaud Coen, M., Guerrero-Rascado, J. L., Costa, M. J., Cimini, D., O'Connor, E. J., Hervo, M., Alados-Arboledas, L., Jiménez-Portaz, M., Mona, L., Ruffieux, D., Illingworth, A., and Haeffelin, M.: Atmospheric boundary layer height from ground-based remote sensing: a review of capabilities and limitations, Atmos. Meas. Tech., 16, 433-479, https://doi.org/10.5194/amt-16-433-2023, 2023.

Kulmala, M.: How Particles Nucleate and Grow, 302, 1000-1001, https://doi.org/10.1126/science.1090848, 2003.

Kulmala, M., Vehkamäki, H., Petäjä, T., Dal Maso, M., Lauri, A., Kerminen, V. M., Birmili, W., and McMurry, P. H.: Formation and growth rates of ultrafine atmospheric particles: a review of observations, J.Aerosol Sci., 35, 143-176, http://dx.doi.org/10.1016/j.jaerosci.2003.10.003, 2004.

Kulmala, M., Aliaga, D., Tuovinen, S., Cai, R., Junninen, H., Yan, C., Bianchi, F., Cheng, Y., Ding, A., Worsnop, D. R., Petäjä, T., Lehtipalo, K., Paasonen, P., and Kerminen, V. M.: Opinion: A paradigm shift in investigating the general characteristics of atmospheric new particle formation using field observations, Aerosol Research, 2, 49-58, https://doi.org/10.5194/ar-2-49-2024, 2024.

Kulmala, M., Petäjä, T., Nieminen, T., Sipilä, M., Manninen, H. E., Lehtipalo, K., Dal Maso, M., Aalto, P. P., Junninen, H., Paasonen, P., Riipinen, I., Lehtinen, K. E. J., Laaksonen, A., and Kerminen, V. M.: Measurement of the nucleation of atmospheric aerosol particles, Nat. Protoc., 7, 1651-1667, https://doi.org/10.1038/nprot.2012.091, 2012.

Lee, S.-H., Gordon, H., Yu, H., Lehtipalo, K., Haley, R., Li, Y., and Zhang, R.: New Particle Formation in the Atmosphere: From Molecular Clusters to Global Climate, J. Geophys. Res.: Atmos., 124, 7098-7146, https://doi.org/10.1029/2018JD029356, 2019.

Leino, K., Lampilahti, J., Poutanen, P., Väänänen, R., Manninen, A., Buenrostro Mazon, S., Dada, L., Franck, A., Wimmer, D., Aalto, P. P., Ahonen, L. R., Enroth, J., Kangasluoma, J., Keronen, P., Korhonen, F., Laakso, H., Matilainen, T., Siivola, E., Manninen, H. E., Lehtipalo, K., Kerminen, V. M., Petäjä, T., and Kulmala, M.: Vertical profiles of sub-3 nm particles over the boreal forest, Atmos. Chem. Phys., 19, 4127-4138, 10.5194/acp-19-4127-2019, 2019.

Lelieveld, J., Klingmüller, K., Pozzer, A., Burnett, R. T., Haines, A., and Ramanathan, V.: Effects of fossil fuel and total anthropogenic emission removal on public health and climate, Proc. Natl. Acad. Sci. 116, 7192-7197, https://doi.org/10.1073/pnas.1819989116, 2019.

Mäkelä, J. M., Riihelä, M., Ukkonen, A., Jokinen, V., and Keskinen, J.: Comparison of mobility equivalent diameter with Kelvin-Thomson diameter using ion mobility data, J. Chem. Phys., 105, 1562-1571, https://doi.org/10.1063/1.472017 , 1996.

Manninen, H. E., Mirme, S., Mirme, A., Petäjä, T., and Kulmala, M.: How to reliably detect molecular clusters and nucleation mode particles with Neutral cluster and Air Ion Spectrometer (NAIS), Atmos. Meas. Tech., 9, 3577-3605, https://doi.org/10.5194/amt-9-3577-2016, 2016.

Manninen, H. E., Nieminen, T., Asmi, E., Gagné, S., Häkkinen, S., Lehtipalo, K., Aalto, P., Vana, M., Mirme, A., Mirme, S., Hõrrak, U., Plass-Dülmer, C., Stange, G., Kiss, G., Hoffer, A., Törő, N., Moerman, M., Henzing, B., de Leeuw, G., Brinkenberg, M., Kouvarakis, G. N., Bougiatioti, A., Mihalopoulos, N., O'Dowd, C., Ceburnis, D., Arneth, A., Svenningsson, B., Swietlicki, E., Tarozzi, L., Decesari, S., Facchini, M. C., Birmili, W., Sonntag, A., Wiedensohler, A., Boulon, J., Sellegri, K., Laj, P., Gysel, M., Bukowiecki, N., Weingartner, E., Wehrle, G., Laaksonen, A., Hamed, A., Joutsensaari, J., Petäjä, T., Kerminen, V.-M., and Kulmala, M.: EUCAARI ion spectrometer measurements at 12 European sites – analysis of new particle formation events, Atmos. Chem. Phys., 10, 7907-7927, https://doi.org/10.5194/acp-10-7907-2010, 2010.

Merikanto, J., Spracklen, D. V., Mann, G. W., Pickering, S. J., and Carslaw, K. S.: Impact of nucleation on global CCN, Atmos. Chem. Phys., 9, 8601-8616, https://doi.org/10.5194/acp-9-8601-2009, 2009.

Minguillón, M. C., Brines, M., Pérez, N., Reche, C., Pandolfi, M., Fonseca, A. S., Amato, F., Alastuey, A., Lyasota, A., Codina, B., Lee, H. K., Eun, H. R., Ahn, K. H., and Querol, X.: New particle formation at ground level and in the vertical column over the Barcelona area, Atmospheric Research, 164-165, 118-130, https://doi.org/10.1016/j.atmosres.2015.05.003, 2015.

Mirme, S. and Mirme, A.: The mathematical principles and design of the NAIS – a spectrometer for the measurement of cluster ion and nanometer aerosol size distributions, Atmos. Meas. Tech., 6, 1061-1071, https://doi.org/10.5194/amt-6-1061-2013, 2013.

Münkel, C. and Roininen, R.: Automatic monitoring of boundary layer structures with ceilometers, Bound.-Lay. Meteorol., 124, 117-128, https://doi.org/10.1007/s10546-006-9103-3, 2010.

Nie, W., Ding, A., Wang, T., Kerminen, V.-M., George, C., Xue, L., Wang, W., Zhang, Q., Petäjä, T., Qi, X., Gao, X., Wang, X., Yang, X., Fu, C., and Kulmala, M.: Polluted dust promotes new particle formation and growth, Scientific Reports, 4, 6634, https://doi.org/10.1038/srep06634, 2014.

Nieminen, T., Asmi, A., Maso, M. D., Aalto, P. P., Keronen, P., Petaja, T., Kulmala, M., and Kerminen, V.-M.: Trends in atmospheric new-particle formation: 16 years of observations in a boreal-forest environment, Boreal Environ. Res., 19, 191-214, ISSN 1797-2469, 2014.

Nieminen, T., Kerminen, V. M., Petäjä, T., Aalto, P. P., Arshinov, M., Asmi, E., Baltensperger, U., Beddows, D. C. S., Beukes, J. P., Collins, D., Ding, A., Harrison, R. M., Henzing, B., Hooda, R., Hu, M., Hõrrak, U., Kivekäs, N., Komsaare, K., Krejci, R., Kristensson, A., Laakso, L., Laaksonen, A., Leaitch, W. R., Lihavainen, H., Mihalopoulos, N., Németh, Z., Nie, W., O'Dowd, C., Salma, I., Sellegri, K., Svenningsson, B., Swietlicki, E., Tunved, P., Ulevicius, V., Vakkari, V., Vana, M., Wiedensohler, A., Wu, Z., Virtanen, A., and Kulmala, M.: Global analysis of continental boundary layer new particle formation based on long-term measurements, Atmos. Chem. Phys., 18, 14737-14756, https://doi.org/10.5194/acp-18-14737-2018, 2018.

O'Donnell, S. E., Akherati, A., He, Y., Hodshire, A. L., Shilling, J. E., Kuang, C., Fast, J. D., Mei, F., Schobesberger, S., Thornton, J. A., Smith, J. N., Jathar, S. H., and Pierce, J. R.: Look Up: Probing the Vertical Profile of New Particle Formation and Growth in the Planetary Boundary Layer With Models and Observations, J. Geophys. Res., 128, e2022JD037525, https://doi.org/10.1029/2022JD037525, 2023.

Pierce, J. R. and Adams, P. J.: Uncertainty in global CCN concentrations from uncertain aerosol nucleation and primary emission rates, Atmos. Chem. Phys., 9, 1339-1356, https://doi.org/10.5194/acp-9-1339-2009, 2009.

Pikridas, M., Riipinen, I., Hildebrandt, L., Kostenidou, E., Manninen, H., Mihalopoulos, N., Kalivitis, N., Burkhart, J. F., Stohl, A., Kulmala, M., and Pandis, S. N.: New particle formation at a remote site in the eastern Mediterranean, J. Geophys. Res., 117, https://doi.org/10.1029/2012JD017570, 2012.

Platis, A., Altstädter, B., Wehner, B., Wildmann, N., Lampert, A., Hermann, M., Birmili, W., and Bange, J.: An Observational Case Study on the Influence of Atmospheric Boundary-Layer Dynamics on New Particle Formation, Boundary-Layer Meteorology, 158, 67-92, https://doi.org/10.1007/s10546-015-0084-y, 2016.

Rose, C., Sellegri, K., Freney, E., Dupuy, R., Colomb, A., Pichon, J. M., Ribeiro, M., Bourianne, T., Burnet, F., and Schwarzenboeck, A.: Airborne measurements of new particle formation in the free troposphere above the Mediterranean Sea during the HYMEX campaign, Atmos. Chem. Phys., 15, 10203-10218, https://doi.org/10.5194/acp-15-10203-2015, 2015.

Schröder, F. and Ström, J.: Aircraft measurements of sub micrometer aerosol particles ( > 7 nm) in the midlatitude free troposphere and tropopause region, Atmospheric Research, 44, 333-356, https://doi.org/10.1016/S0169-8095(96)00034-8, 1997.

Sebastian, M., Kanawade, V. P., Soni, V., Asmi, E., Westervelt, D. M., Vakkari, V., Hyvärinen, A. P., Pierce, J. R., and Hooda, R. K.: New Particle Formation and Growth to Climate-Relevant Aerosols at a Background Remote Site in the Western Himalaya, J. Geophys. Res., 126, e2020JD033267, https://doi.org/10.1029/2020JD033267, 2021.

Sebastian, M., Kompalli, S. K., Kumar, V. A., Jose, S., Babu, S. S., Pandithurai, G., Singh, S., Hooda, R. K., Soni, V. K., Pierce, J. R., Vakkari, V., Asmi, E., Westervelt, D. M., Hyvärinen, A. P., and Kanawade, V. P.: Observations of particle number size distributions and new particle formation in six Indian locations, Atmos. Chem. Phys., 22, 4491-4508, https://doi.org/10.5194/acp-22-4491-2022, 2022.

Sellegri, K., Rose, C., Marinoni, A., Lupi, A., Wiedensohler, A., Andrade, M., Bonasoni, P., and Laj, P.: New Particle Formation: A Review of Ground-Based Observations at Mountain Research Stations, Atmosphere, 10, 493, https://doi.org/10.3390/atmos10090493, 2019.

Spracklen, D. V., Carslaw, K. S., Kulmala, M., Kerminen, V.-M., Sihto, S.-L., Riipinen, I., Merikanto, J., Mann, G. W., Chipperfield, M. P., Wiedensohler, A., Birmili, W., and Lihavainen, H.: Contribution of particle formation to global cloud condensation nuclei concentrations, Geophys. Res. Lett., 35, 2007GL033038, https://doi.org/10.1029/2007gl033038, 2008.

Stratmann, F., Siebert, H., Spindler, G., Wehner, B., Althausen, D., Heintzenberg, J., Hellmuth, O., Rinke, R., Schmieder, U., Seidel, C., Tuch, T., Uhrner, U., Wiedensohler, A., Wandinger, U., Wendisch, M., Schell, D., and Stohl, A.: New-particle formation events in a continental boundary layer: first results from the SATURN experiment, Atmos. Chem. Phys., 3, 1445-1459, https://doi.org/10.5194/acp-3-1445-2003, 2003.

Stull, R. B.: An Introduction to Boundary Layer Meteorology, Atmospheric and Oceanographic Sciences Library, Springer Dordrecht, https://doi.org/10.1007/978-94-009-3027-8, 1988.

Tröstl, J., Herrmann, E., Frege, C., Bianchi, F., Molteni, U., Bukowiecki, N., Hoyle, C. R., Steinbacher, M., Weingartner, E., Dommen, J., Gysel, M., and Baltensperger, U.: Contribution of new particle formation to the total aerosol concentration at the high-altitude site Jungfraujoch (3580 m asl, Switzerland), J. Geophys. Res., 121, 11,692-611,711, https://doi.org/10.1002/2015jd024637, 2016a.

Tröstl, J., Chuang, W. K., Gordon, H., Heinritzi, M., Yan, C., Molteni, U., Ahlm, L., Frege, C., Bianchi, F., Wagner, R., Simon, M., Lehtipalo, K., Williamson, C. J., Craven, J. S., Duplissy, J., Adamov, A., Almeida, J., Bernhammer, A. K., Breitenlechner, M., Brilke, S., Dias, A., Ehrhart, S., Flagan, R. C., Franchin, A., Fuchs, C., Guida, R., Gysel, M., Hansel, A., Hoyle, C. R., Jokinen, T., Junninen, H., Kangasluoma, J., Keskinen, H., Kim, J., Krapf, M., Kürten, A., Laaksonen, A., Lawler, M. J., Leiminger, M., Mathot, S., Möhler, O., Nieminen, T., Onnela, A., Petäjä, T., Piel, F. M., Miettinen, P., Rissanen, M. P., Rondo, L., Sarnela, N., Schobesberger, S., Sengupta, K., Sipilä, M., Smith, J. N., Steiner, G., Tomè, A., Virtanen, A., Wagner, A. C., Weingartner, E., Wimmer, D., Winkler, P. M., Ye, P., Carslaw, K. S., Curtius, J., Dommen, J., Kirkby, J., Kulmala, M., Riipinen, I., Worsnop, D. R., Donahue, N. M., and Baltensperger, U.: The role of low-volatility organic compounds in initial particle growth in the atmosphere, Nature, 533, 527-531, https://doi.org/10.1038/nature18271, 2016b.

Vrekoussis, M., Pikridas, M., Rousogenous, C., Christodoulou, A., Desservettaz, M., Sciare, J., Richter, A., Bougoudis, I., Savvides, C., and Papadopoulos, C.: Local and regional air pollution characteristics in Cyprus: A long-term trace gases observations analysis, Sci. Total Environ., 845, 157315, https://doi.org/10.1016/j.scitotenv.2022.157315, 2022.

Wang, M. and Penner, J. E.: Aerosol indirect forcing in a global model with particle nucleation, Atmos. Chem. Phys., 9, 239-260, https://doi.org/10.5194/acp-9-239-2009, 2009.

Wehner, B., Werner, F., Ditas, F., Shaw, R. A., Kulmala, M., and Siebert, H.: Observations of new particle formation in enhanced UV irradiance zones near cumulus clouds, Atmos. Chem. Phys., 15, 11701-11711, https://doi.org/10.5194/acp-15-11701-2015, 2015.

Wehner, B., Siebert, H., Ansmann, A., Ditas, F., Seifert, P., Stratmann, F., Wiedensohler, A., Apituley, A., Shaw, R. A., Manninen, H. E., and Kulmala, M.: Observations of turbulence-induced new particle formation in the residual layer, Atmos. Chem. Phys., 10, 4319-4330, https://doi.org/10.5194/acp-10-4319-2010, 2010.

Westervelt, D. M., Pierce, J. R., and Adams, P. J.: Analysis of feedbacks between nucleation rate, survival probability and cloud condensation nuclei formation, Atmos. Chem. Phys., 14, 5577-5597, https://doi.org/10.5194/acp-14-5577-2014, 2014.

Westervelt, D. M., Pierce, J. R., Riipinen, I., Trivitayanurak, W., Hamed, A., Kulmala, M., Laaksonen, A., Decesari, S., and Adams, P. J.: Formation and growth of nucleated particles into cloud condensation nuclei: model–measurement comparison, Atmos. Chem. Phys., 13, 7645-7663, https://doi.org/10.5194/acp-13-7645-2013, 2013.

Williamson, C. J., Kupc, A., Axisa, D., Bilsback, K. R., Bui, T., Campuzano-Jost, P., Dollner, M., Froyd, K. D., Hodshire, A. L., Jimenez, J. L., Kodros, J. K., Luo, G., Murphy, D. M., Nault, B. A., Ray, E. A., Weinzierl, B., Wilson, J. C., Yu, F., Yu, P., Pierce, J. R., and Brock, C. A.: A large source of cloud condensation nuclei from new particle formation in the tropics, Nature, 574, 399-403, https://doi.org/10.1038/s41586-019-1638-9, 2019.

Yu, F. and Luo, G.: Simulation of particle size distribution with a global aerosol model: contribution of nucleation to aerosol and CCN number concentrations, Atmos. Chem. Phys., 9, 7691-7710, https://doi.org/10.5194/acp-9-7691-2009, 2009.

Zha, Q., Aliaga, D., Krejci, R., Sinclair, V. A., Wu, C., Ciarelli, G., Scholz, W., Heikkinen, L., Partoll, E., Gramlich, Y., Huang, W., Leiminger, M., Enroth, J., Peräkylä, O., Cai, R., Chen, X., Koenig, A. M., Velarde, F., Moreno, I., Petäjä, T., Artaxo, P., Laj, P., Hansel, A., Carbone, S., Kulmala, M., Andrade, M., Worsnop, D., Mohr, C., and Bianchi, F.: Oxidized organic molecules in the tropical free troposphere over Amazonia, National Science Review, 11, https://doi.org/10.1093/nsr/nwad138, 2023.

Zhang, D., Comstock, J., and Morris, V.: Comparison of planetary boundary layer height from ceilometer with ARM radiosonde data, Atmos. Meas. Tech., 15, 4735-4749, https://doi.org/10.5194/amt-15-4735-2022, 2022.

Zhang, R., Suh, I., Zhao, J., Zhang, D., Fortner, E. C., Tie, X., Molina, L. T., and Molina, M. J.: Atmospheric New Particle Formation Enhanced by Organic Acids, Science, 304, 1487-1490, https://doi.org/10.1126/science.1095139, 2004.

Zittis, G., Almazroui, M., Alpert, P., Ciais, P., Cramer, W., Dahdal, Y., Fnais, M., Francis, D., Hadjinicolaou, P., Howari, F., Jrrar, A., Kaskaoutis, D. G., Kulmala, M., Lazoglou, G., Mihalopoulos, N., Lin, X., Rudich, Y., Sciare, J., Stenchikov, G., Xoplaki, E., and Lelieveld, J.: Climate Change and Weather Extremes in the Eastern Mediterranean and Middle East, Rev. Geophys., 60, e2021RG000762, https://doi.org/10.1029/2021R, G000762, 2022.